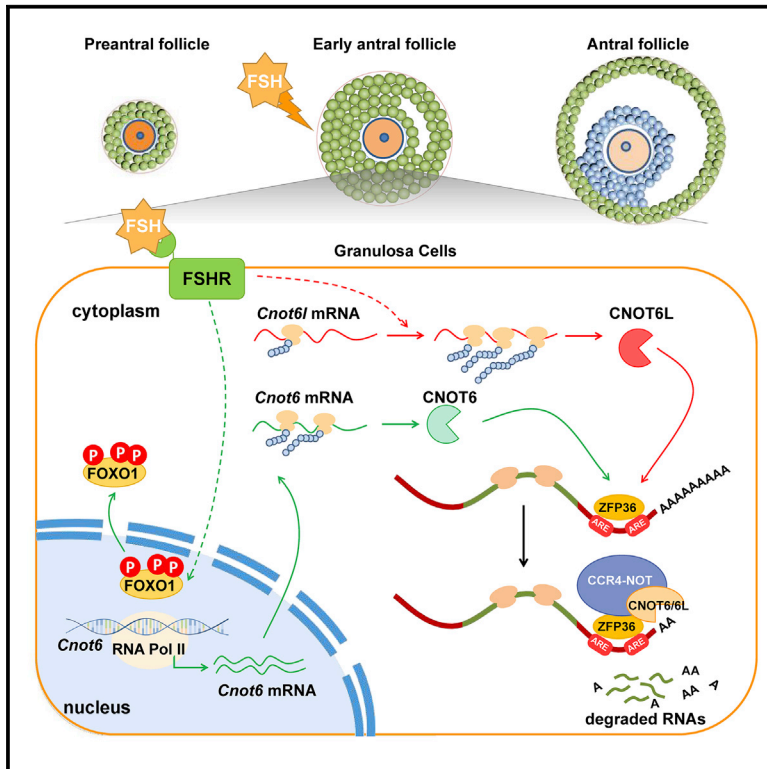


CNOT6/6L-mediated mRNA degradation in ovarian granulosa cells is a key mechanism of gonadotropin-triggered follicle development

Graphical abstract



Authors

Xing-Xing Dai, Zhi-Yan Jiang, Yun-Wen Wu, ..., Wen-Dong Xi, Jing Li, Heng-Yu Fan

Correspondence

hyfan@zju.edu.cn

In brief

Dai et al. report that the CNOT6/6L subunit of the CCR4-NOT complex is downstream effectors of the pituitary gonadotropin follicle-stimulating hormone (FSH) in ovarian granulosa cells. CNOT6/6L catalyzes the deadenylation and degradation of a broad spectrum of transcripts encoding factors that repress follicle growth and endocrine activities.

Highlights

- mRNA deadenylation is essential for female reproductive endocrine regulation
- CNOT6/6L are specific molecular targets of FSH in granulosa cells
- FSH-induced clearance of a subset of mRNAs in granulosa cells is CNOT6/6L dependent
- The CCR4-NOT^{CNOT6/6L} deadenylase are indispensable in female reproduction



Article

CNOT6/6L-mediated mRNA degradation in ovarian granulosa cells is a key mechanism of gonadotropin-triggered follicle development

Xing-Xing Dai,^{1,5} Zhi-Yan Jiang,^{1,5} Yun-Wen Wu,¹ Qian-Qian Sha,² Yang Liu,³ Jia-Yi Ding,³ Wen-Dong Xi,⁴ Jing Li,⁴ and Heng-Yu Fan^{1,6,*}

¹Life Sciences Institute, Zhejiang University, Hangzhou 310058, China

²Fertility Preservation Laboratory, Reproductive Medicine Center, Guangdong Second Provincial General Hospital, Guangzhou 510317, China

³Department of Assisted Reproduction, Affiliated Maternity and Child Health Care Hospital of Nantong University, Nantong 226000, China

⁴State Key Laboratory of Reproductive Medicine, Nanjing Medical University, Nanjing 211100, China

⁵These authors contributed equally

⁶Lead contact

*Correspondence: hyfan@zju.edu.cn

<https://doi.org/10.1016/j.celrep.2021.110007>

SUMMARY

CCR4-NOT deadenylase is a major regulator of mRNA turnover. It contains two heterogeneous catalytic subunits CNOT7/8 and CNOT6/6L in vertebrates. The physiological function of each catalytic subunit is unclear due to the gene redundancy. In this study, *Cnot6/6l* double knockout mice are generated. *Cnot6/6l*^{-/-} female mice are infertile, with poor ovarian responses to gonadotropins. Follicle-stimulating hormone (FSH) stimulates the transcription and translation of *Cnot6* and *Cnot6l* in ovarian granulosa cells. CNOT6/6L function as key effectors of FSH in granulosa cells and trigger the clearance of specific transcripts in granulosa cells during preantral to antral follicle transition. These results demonstrate that FSH modulates granulosa cell function by stimulating selective translational activation and degradation of existing mRNAs, in addition to inducing *de novo* gene transcription. Meanwhile, this study provides *in vivo* evidence that CNOT6/6L-mediated mRNA deadenylation is dispensable in most somatic cell types, but is essential for female reproductive endocrine regulation.

INTRODUCTION

Deadenylation is an initial step in cytoplasmic mRNA turnover (Wiederhold and Passmore, 2010). An important enzyme complex involved in poly(A) shortening is the CCR4-NOT deadenylase (Dojige et al., 2012; Temme et al., 2014). In addition to at least 6 regulatory subunits, the vertebrate CCR4-NOT complex contains 1 DEDD (Asp-Glu-Asp-Asp)-type deadenylase, which is either CNOT7 or CNOT8, and 1 endonuclease-exonuclease-phosphatase (EEP)-type ribonuclease, either CNOT6 or CNOT6L (Aslam et al., 2009; Maryati et al., 2014; Winkler and Balacco, 2013).

In mammals, the physiological importance of CCR4-NOT-mediated mRNA deadenylation has only been demonstrated in spermatocytes, oocytes, and zygotes (Gou et al., 2014; Sha et al., 2018; Yu et al., 2016). These cell types are ideal model systems for studying mRNA post-transcriptional regulation because genome transcription activity is silenced during the late stage of germ cell development and early embryogenesis. *Cnot7*^{-/-} male mice are sterile, and the onset of the defect occurs during the first wave of spermatogenesis after birth (i.e., during meiotic progression of pachytene spermatocytes to haploid spermatids

and spermatozoa) (Berthet et al., 2004). In contrast, *Cnot6l* is predominantly expressed in mouse oocytes and plays a major role in mediating maternal mRNA deadenylation during meiotic maturation and maternal-to-zygotic transition (Berthet et al., 2004; Sha et al., 2018). However, the function of CCR4-NOT may not be restricted to germ cells and zygotes. Global profiling of transcriptomes in *Cnot7/8*- or *Cnot6/6l*-depleted cell lines has revealed the role of the CCR4-NOT complex as a predominant and general mRNA deadenylase (Mostafa et al., 2020). Nevertheless, genetic evidence showing the *in vivo* function of CCR4-NOT in regulating mRNA stability is lacking in mammalian somatic cells.

In this study, we generated *Cnot6/6l* double knockout mice and demonstrated that CNOT6/6L is a downstream effector of follicle-stimulating hormone (FSH) in granulosa cells (GCs). In addition to inducing the transcription of *Cnot6/6l* genes, FSH also triggered the translation of mRNAs encoding CNOT6/6L. In return, CNOT6/6L catalyzed deadenylation and degradation of a broad spectrum of transcripts encoding factors that repressed follicle growth and endocrine activities, including anti-Müllerian hormone (AMH) and FOXO1, an inhibitory transcriptional factor that restricts proestrus follicle growth and steroidogenesis (Liu et al., 2013). This was a previously



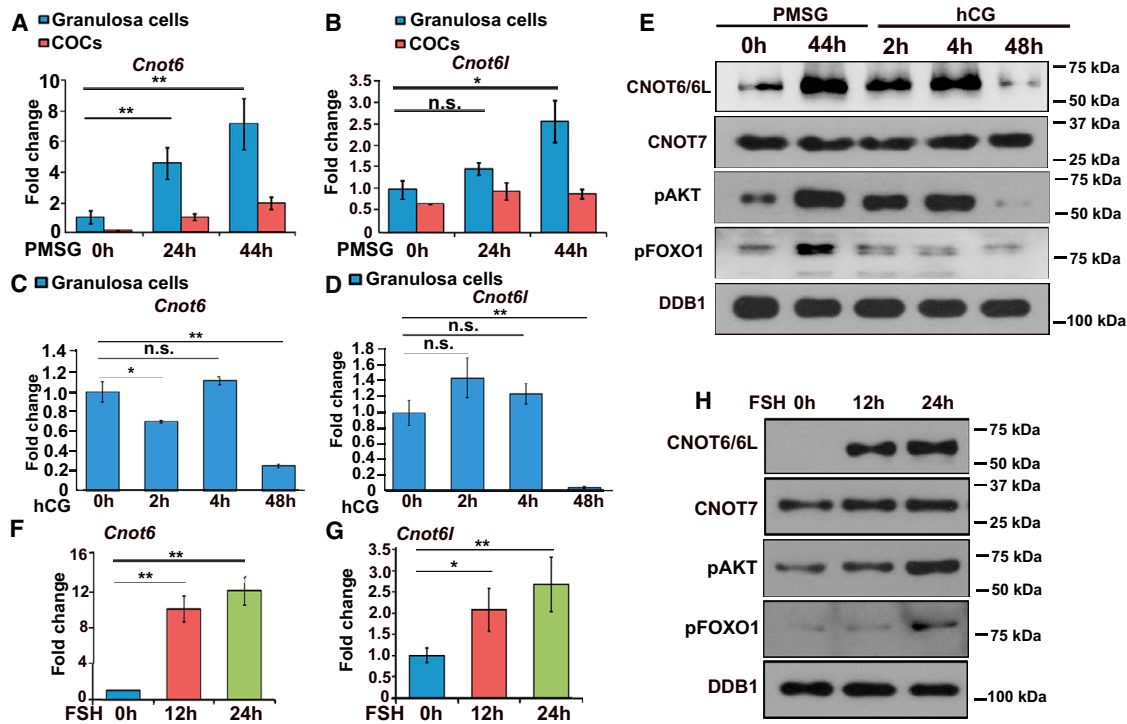


Figure 1. FSH induces the rapid accumulation of CNOT6/6L in granulosa cells (GCs)

(A and B) *Cnot6* (A) and *Cnot6l* (B) expression levels through quantitative RT-PCR (qRT-PCR) in GCs and cumulus-oocyte complexes (COCs) isolated from wild-type (WT) ovaries after pregnant mare serum gonadotropin (PMSG). Error bars indicate SEMs. Data are presented as the means \pm SEMs from at least 3 independent experiments, 1-way ANOVA, * $p < 0.05$, ** $p < 0.01$; n.s., nonsignificant.

(C and D) *Cnot6* (C) and *Cnot6l* (D) expression levels through qRT-PCR in GCs isolated from WT ovaries after hCG (0, 2, 4, and 48 h). Error bars indicate SEMs. Data are presented as the means \pm SEMs from at least 3 independent experiments, 1-way ANOVA, * $p < 0.05$, ** $p < 0.01$.

(E) Western blotting shows the expression levels of CNOT6/6L and CNOT7 proteins, phosphorylated AKT, and FOXO1 in ovarian lysates in WT mice before and after PMSG and hCG treatments. Endogenous DDB1 was used as a loading control.

(F and G) qRT-PCR shows *Cnot6* (F) and *Cnot6l* (G) mRNA expression levels in cultured GCs treated with follicle-stimulating hormone (FSH) (100 ng/mL). Error bars indicate SEMs. Data are presented as the means \pm SEMs from at least 3 independent experiments, 1-way ANOVA, * $p < 0.05$, ** $p < 0.01$.

(H) Western blotting shows the expression levels of CNOT and FOXO1 proteins in cultured GCs treated with FSH (100 ng/mL). Endogenous DDB1 was used as a loading control.

unrecognized mechanism that mediates the physiological function of FSH. Conceptually, this study reveals an additional layer of regulation mechanism—that is, regulating mRNA stability underlying gonadotropin functions—and provides *in vivo* evidence that CCR4-NOT^{CNOT6/6L}-mediated mRNA deadenylation is essential in some but not all somatic cell types.

RESULTS

Cnot6 and *Cnot6l* are FSH downstream genes in GCs

When mice were injected with pregnant mare serum gonadotropin (PMSG) to induce rapid follicle growth, the mRNA level of *Cnot6* significantly increased in GCs (Figure 1A). PMSG mimicked FSH functions and stimulated follicle growth. *Cnot6l* mRNA levels also modestly increased after PMSG treatment, but not as significantly as that of *Cnot6* (Figure 1B). Both *Cnot6* and *Cnot6l* have higher expression levels in GCs than in cumulus-oocyte complexes (COCs) (Figures 1A and 1B). An injection of human chorionic gonadotropin (hCG) at 44 h after PMSG treatment did not further increase the expression levels

of *Cnot6/6l* in GCs (Figures 1C and 1D). *Cnot6/6l* mRNA levels decreased in luteal cells at 48 h after hCG injection. Consistent with the quantitative RT-PCR (qRT-PCR) results, CNOT6/6L protein expression was induced by PMSG treatment, maintained at a high level after hCG injection, and decreased 48 h later (Figure 1E). In contrast, CNOT7 was continuously expressed in GCs before and after PMSG and hCG treatments (Figure 1E). The intensities of indicated bands normalized by the DDB1 (a protein strong and stably expressed in GCs as a loading control) bands in the same samples was quantified (Figure S1A).

To investigate whether FSH directly stimulated CNOT6/6L expression, we isolated and cultured primary GCs and then treated them with FSH. The *Cnot6/6l* mRNA levels (Figures 1F and 1G) and CNOT6/6L protein levels (Figures 1H and S1B) significantly increased after FSH treatment, while the CNOT7 protein level remained stable (Figures 1H and S1B). The accumulation of CNOT6/6L in GCs after PMSG and FSH treatments suggested that they are FSH-downstream targets and potentially play an important role in the growth and differentiation of GCs during follicle development.

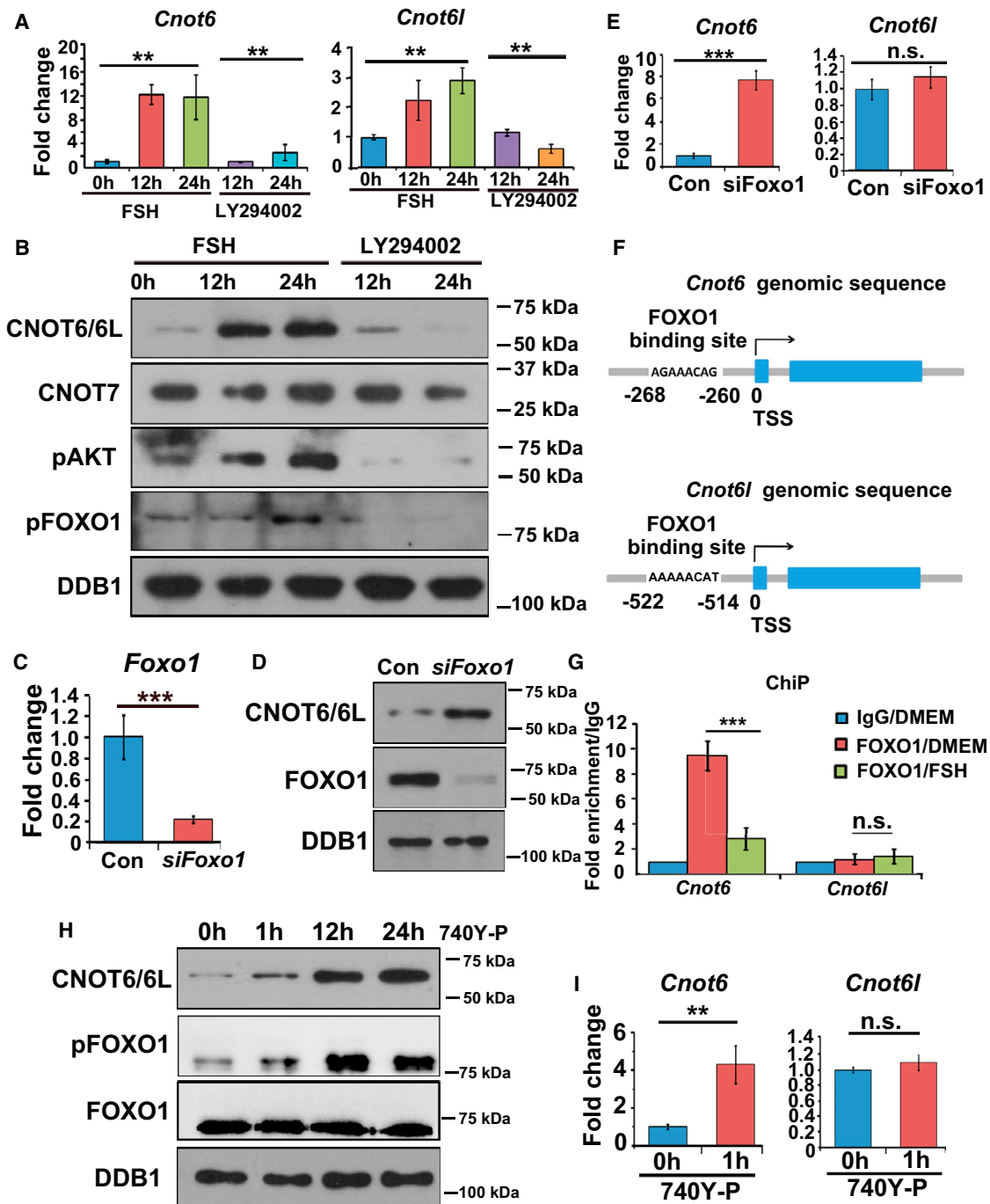


Figure 2. PI3K signaling pathway regulates the expression of *Cnot6* in GCs

(A) *Cnot6/6l* expression in cultured GCs treated with FSH (100 ng/mL) and the PI3K inhibitor LY294002 (10 μM) through qRT-PCR. Error bars indicate SEMs. Data are presented as the means ± SEMs from at least 3 independent experiments, 1-way ANOVA, **p < 0.01.

(B) Western blotting shows the CNOT6/6L and CNOT7 expression levels in cultured GCs treated with FSH and LY294002. Endogenous DDB1 was used as a loading control.

(C and D) qRT-PCR (C) and western blotting (D) results shows the deletion effect of *Foxo1* through RNA interference (*siFoxo1*). Error bars indicate SEMs. ***p < 0.001 as determined through 2-tailed Student's t test.

(E) qRT-PCR results show the *Cnot6/6l* expression levels in GCs with or without *Foxo1* depletion. Error bars indicate SEMs. ***p < 0.001 as determined through 2-tailed Student's t test.

(F) Putative FOXO1-binding sequences in the promoters of mouse *Cnot6* and *Cnot6l* genes. TSS, transcription start site.

(legend continued on next page)

FSH induces *Cnot6* mRNA expression in GCs by activating the PI3K/AKT pathway

The phosphoinositide 3-kinase (PI3K) signaling pathway is a key mediator of FSH function in GCs (Fan et al., 2008). The downstream effectors of PI3K, including AKT and FOXO1, were transiently phosphorylated in GCs after PMSG and hCG injections *in vivo* (Figures 1E and S1A) and FSH treatment *in vitro* (Figures 1H and S1B). The activation window of the PI3K pathway overlaps with that of CNOT6/6L expression. When cultured GCs were treated with the PI3K inhibitor LY294002, both *Cnot6/6l* mRNA and CNOT6/6L protein expression failed to be induced after FSH treatment (Figures 2A, 2B, and S1C). These results indicated that the transient CNOT6/6L accumulation in the growing GCs was due to the FSH-activated PI3K signaling pathway.

During preantral-to-antral follicle transition, FSH relieves the repressing effect of FOXO1 on GC proliferation and steroidogenesis by inducing FOXO1 phosphorylation through the PI3K/AKT pathway and translocation from the nucleus to the cytoplasm (Liu et al., 2015). To examine whether the expression of *Cnot6/6l* was also regulated by this mechanism, we depleted *Foxo1* in cultured GCs through small interfering RNA (siRNA)-mediated RNA interference (RNAi) (Figures 2C, 2D, and S1D). After *Foxo1* knockdown, *Cnot6* transcription remarkably increased, while the mRNA level of *Cnot6l* was not affected (Figure 2E). The CNOT6/6L total protein level was also increased in FOXO1-depleted GCs (Figure 2D). Furthermore, we performed chromatin immunoprecipitation to test whether FOXO1 binds to *Cnot6/6l* promoters (Brind'Amour et al., 2015). Primers targeting the putative FOXO1 binding motif on the promoters of mouse *Cnot6* and *Cnot6l* were used for qRT-PCRs (Figure 2F). The results indicated that FOXO1 interacted with the *Cnot6* promoter but not with the *Cnot6l* promoter (Figure 2G), and were consistent with the observation that *Foxo1* depletion derepressed the expression of *Cnot6*, but not that of *Cnot6l*. The binding affinity between FOXO1 and *Cnot6* decreased after FSH treatment, suggesting that FSH triggered *Cnot6* expression by releasing FOXO1 from the *Cnot6* promoter (Figure 2G).

Following this, we determined whether the PI3K pathway was sufficient to induce *Cnot6/6l* expression by treating cultured GCs with 740Y-P (20 nM), an activator of the PI3K signaling pathway (Sun et al., 2015). AKT phosphorylation was detected as early as 0.5 h post-740Y-P addition (Figure S2A). Immunofluorescence showed that FOXO1 was mainly located in the nucleus of untreated GCs, but translocated to the cytoplasm after 740Y-P treatment (Figure S2B). Although the total FOXO1 protein level did not change after 740Y-P treatment, phosphorylated FOXO1 accumulated in 740Y-P treated GCs (Figures 2H, S1E, and S2C). These results showed that 740Y-P effectively activated the PI3K signaling pathway in GCs. After 740Y-P addition to cultured GCs, the mRNA levels of *Cnot6* increased rapidly,

while *Cnot6l* did not change (Figure 2I). CNOT6/6L protein levels also increased (Figures 2H and S1E).

FSH induces the translational activation of *Cnot6l* transcripts in GCs by regulating its 3' untranslated region (3' UTR)

Cnot6l transcription did not increase as much as *Cnot6* after FSH treatment and was not regulated by FOXO1 (Figure 2I). However, PMSG injection *in vivo* and FSH treatment *in vitro* still stimulated the accumulation of CNOT6L in GCs of *Cnot6* null mice, as described later (Figures 3A and 3B). To validate whether the FSH-induced CNOT6L increase was based on translational activation, we constructed a reporter plasmid in which the expression of FLAG-GFP was regulated by mouse *Cnot6l* 3' UTR (FLAG-*Gfp*-3' UTR_{*Cnot6l*}) and transfected into GCs (Figure 3C). Its expression was stimulated by FSH but was repressed by the PI3K inhibitor LY294002 (Figures 3D and 3E). An mCherry-expressing plasmid containing an SV40 3' UTR was co-transfected as a control. Its expression was consistent and did not differ among these groups (Figure 3D). Furthermore, when *Cnot6l* mRNA transcription in GCs was blocked by the RNA polymerase II inhibitor α -amanitin (50 μ M) (Figures 3B and S2D), FSH still increased CNOT6L protein levels in *Cnot6* null GCs (Figures 3B and S1G). These results indicate that FSH promotes the translation of preexisting *Cnot6l* transcripts, resulting in CNOT6/6L protein accumulation.

CNOT6/6L in GCs were required for FSH-induced preantral-to-antral follicle transition

To investigate the *in vivo* function of CNOT6 and its potential redundancy with CNOT6L, we generated a *Cnot6* knockout mouse strain. This strain contained a deletion of exon 3 (86 bp) and caused a reading frameshift. *Cnot6*^{-/-} female mice were generally healthy and fertile, and had normal body, uterus, and ovarian sizes (Figures S3A–S3C). *Cnot6*^{-/-} female mice also had normal ovarian morphology, with the presence of developing follicles and all different stages (Figure S3D). These results suggested that *Cnot6* was not an essential gene in mice.

Previous studies reported that *Cnot6l*^{-/-} mice were viable but that females were subfertile (Horvat et al., 2018; Sha et al., 2018). Therefore, we generated *Cnot6*^{-/-} and *Cnot6l*^{-/-} double knockout (*Cnot6/6l*^{-/-}) mice to evaluate the potential redundant function of these two genes. The *Cnot6/6l*^{-/-} mice developed into adulthood without apparent defects, except that females were sterile. As there are no commercial antibodies that specifically recognize CNOT6 or CNOT6L, we used an antibody that targeted both CNOT6 and CNOT6L in western blotting. The results showed that the levels of CNOT6 in *Cnot6l*^{-/-} ovaries and CNOT6L in *Cnot6*^{-/-} ovaries were comparable, and each was half the CNOT6/6L level in the wild-type (WT) ovaries (Figure 4A). However, CNOT6/6L were completely absent in the ovarian

(G) Chromatin immunoprecipitation (ChIP) and qRT-PCR results showing the enrichment of *Cnot6* and *Cnot6l* promoter fragments through FOXO1 antibody and control rabbit immunoglobulin G (IgG). Error bars indicate SEMs. ***p < 0.001 as determined through 2-tailed Student's t test.

(H) Western blotting shows CNOT6/6L, pFOXO1, and FOXO1 expression levels in cultured GCs treated with 740Y-P (20 nM). Endogenous DDB1 was used as a loading control.

(I) qRT-PCR results show *Cnot6* and *Cnot6l* expression levels in GCs with or without 740Y-P treatment. Error bars indicate SEMs. **p < 0.01 as determined through 2-tailed Student's t test.

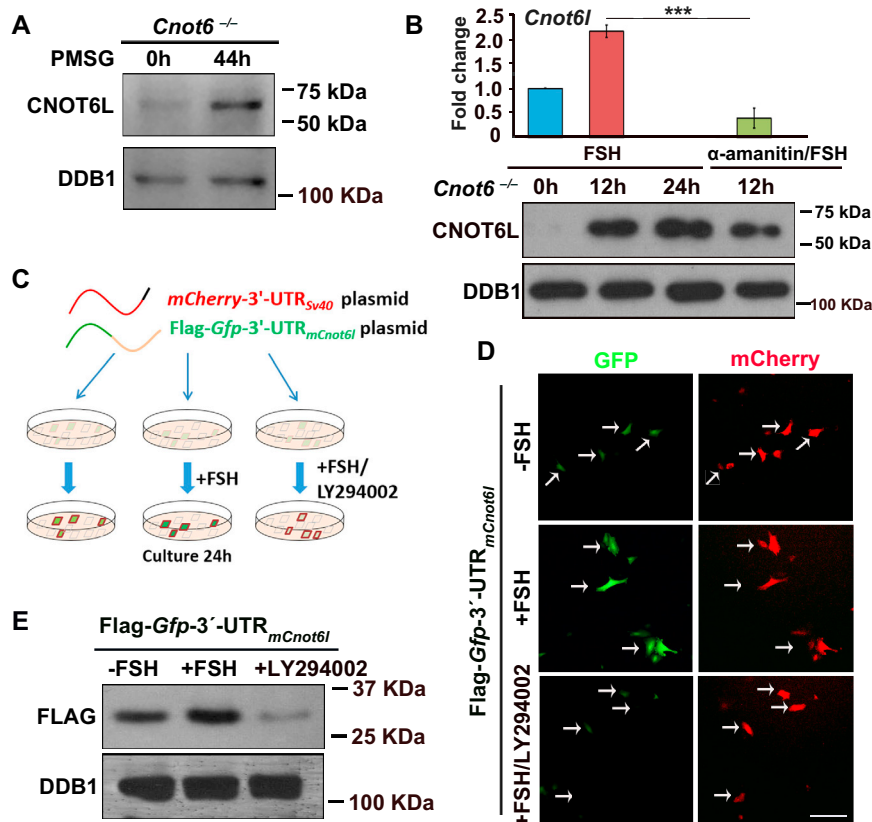


Figure 3. FSH promotes the translation of *Cnot6l* transcript in GCs

(A) Western blotting shows CNOT6L expression levels in GCs isolated from *Cnot6*^{-/-} female mice with or without PMSG treatment for 44 h. Endogenous DDB1 was used as a loading control. (B) qRT-PCR and western blotting shows *Cnot6l* mRNA and CNOT6L/6L protein expression levels in cultured *Cnot6*^{-/-} GCs treated with FSH (100 ng/mL) or FSH plus α -amanitin (50 μ M). Error bars indicate SEMs. ***p < 0.001 as determined through 2-tailed Student's t test. (C) Illustration of plasmid transfection, GC culture, and treatment in (D) and (E). (D and E) Fluorescence microscopy (D) and western blotting (E) results show the expression levels of FLAG-GFP driven by *Cnot6l*-3' UTRs in GCs treated with FSH (100 ng/mL) or FSH plus LY294002 (20 μ M). Arrows indicate transfected cells.

Cnot6l^{-/-} mice also had significantly lower serum estrogen levels compared to those of WT mice, after 44 h of PMSG treatment (Figure 5B). Four-week-old *Cnot6l*^{-/-} mice after PMSG treatment had fewer dividing GCs labeled with phosphorylated histone H3 at serine 10 (a mitotic cell marker) in growing follicles than those of WT mice (Figures 5D and 5E). We also detected cleaved caspase 3

lysates of *Cnot6l*^{-/-} mice (Figure 4A). In contrast, CNOT7 levels were unaffected by the *Cnot6l* knockout.

The ovaries of 4-week-old *Cnot6l*^{-/-} mice injected with PMSG for 44 h were smaller than those of WT control mice (Figures 4B and 4C). The 8-week-old and 6-month-old *Cnot6l*^{-/-} female mice also presented with smaller ovaries than those of WT mice of the same age (Figures 4B and 4C). Ovarian histological analysis of postnatal mice indicated that the *Cnot6l*^{-/-} females had a similar number of primordial follicles, in which oocytes were surrounded with flattened, squamous GCs (Figure 4D). In the ovaries of 4-week (PMSG treated) and 8-week-old *Cnot6l*^{-/-} female mice, the numbers of primary and secondary follicles were similar to those in WT mice, but the number of antral follicles was lower than that in control mice (Figures 4E–4H). We also calculated the ratio of late secondary follicles to antral follicles at 4 weeks (PMSG treated) and 8 weeks of age, and found that the ratio in *Cnot6l*^{-/-} mice was significantly higher than that in WT mice (Figure 4I). This phenomenon indicated that CNOT6 and CNOT6L deletion affected the transition from secondary to antral follicles.

FSH and luteinizing hormone (LH)-induced cellular and molecular events in GCs are impaired in *Cnot6l*^{-/-} mice

Disordered estrous cycles (Figures 5A and S3E) and significant decreases in estrogen and progesterone levels (Figures 5B and 5C) were found in 8-week-old *Cnot6l*^{-/-} mice. The 4-week-old

(CC3, a marker of apoptosis) through immunohistochemistry (IHC) and found a greater number of apoptotic GCs in follicles of PMSG-treated 4-week-old *Cnot6l*^{-/-} mice (Figures 5F and 5G). The Cell Counting Kit-8 (CCK-8) was used to detect the *in vitro* proliferation of GCs isolated from WT and *Cnot6l*^{-/-} mice. The results showed that the proliferation of *Cnot6l*^{-/-} GCs was slower than that of the WT GCs (Figure 5H). Adding FSH to the culture medium stimulated the proliferation of WT GCs. However, the growth rate of *Cnot6l*^{-/-} GCs was still slower than that of WT cells (Figure 5H).

Moreover, the transcription of FSH target genes, including *Fshr* and *Lhcgr* (which encode FSH and LH receptors, respectively) (Fan et al., 2010), *Cyp19a1*, *Cyp11a1*, *Star* (which encode key proteins of steroidogenesis) (Parakh et al., 2006), and *Sfrp4* (which encodes secreted Frizzled-related protein 4, a regulator of the WNT signaling pathway) (Hossein et al., 2016; Hsieh et al., 2003) were induced in GCs of WT mice following PMSG treatment (Manna et al., 2016). However, the inducing effect of PMSG was significantly compromised in the GCs of *Cnot6l*^{-/-} mice (Figure 5I).

When the PMSG-primed female mice were further treated with hCG, which mimics LH function *in vivo*, ~60 mature oocytes were ovulated by the WT mice, but only one-third of the oocytes were ovulated by the *Cnot6l*^{-/-} mice on average (Figure S4A). After the superovulation treatment, the ovaries of *Cnot6l*^{-/-} mice were smaller than those of WT mice (Figures S4B and S4C). Cumulus expansion was significantly impaired in

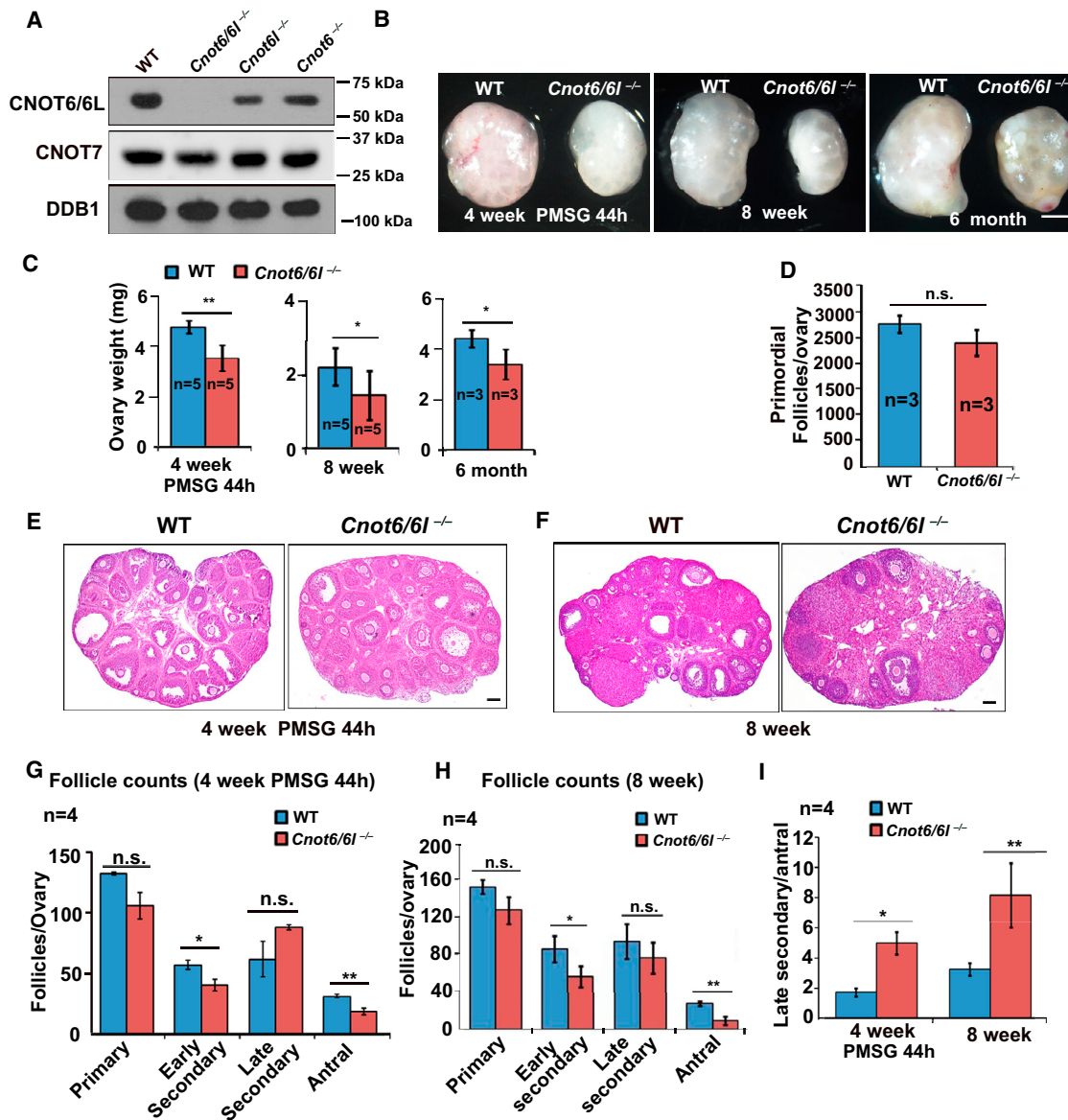


Figure 4. *Cnot6/6l^{-/-}* female mice present defects in follicular development

(A) Western blotting shows the expression levels of CNOT6/6L and CNOT7 proteins in ovarian lysates of WT, *Cnot6^{-/-}*, *Cnot6l^{-/-}*, and *Cnot6/6l^{-/-}* mice 44 h after PMSG injection. Endogenous DDB1 was used as a loading control.

(B and C) Representative ovarian images (B) and weights (C) of WT and *Cnot6/6l^{-/-}* female mice at the indicated ages. n, number of mice analyzed for each genotype. Scale bar, 500 μ m.

(D) Average numbers of primordial follicles in 7-day-old WT and *Cnot6/6l^{-/-}* mice.

(E and F) H&E staining results showing ovarian histology of WT and *Cnot6/6l^{-/-}* female mice at the indicated ages. Scale bar, 100 μ m.

(G and H) Average numbers of primary, secondary, and antral follicles in ovaries of WT and *Cnot6/6l^{-/-}* female mice at the indicated ages.

(I) Ratio of preantral follicles to antral follicles in ovaries of WT and *Cnot6/6l^{-/-}* female mice at the indicated ages. Error bars indicate SEMs; * $p < 0.05$, ** $p < 0.01$ as determined through 2-tailed Student's t test; H&E, hematoxylin and eosin.

the preovulatory follicles of *Cnot6/6l^{-/-}* mice when compared with those in WT mice (Figure S4D). Subsequently, preovulatory follicles did not rupture at 16 h after hCG injection (Figure S4D). Previous studies have shown that the mitogen-activated protein kinase (MAPK) cascade and its targeted transcription factor $CEBP\alpha/\beta$ constitute a crucial signaling pathway that mediates the ovulation signal of LH (Fan et al., 2009, 2011). Immunofluo-

rescence results showed that there was less ERK1/2 phosphorylation and $CEBP\alpha$ expression in the preovulatory follicles of 4-week-old *Cnot6/6l^{-/-}* mice after hCG treatment (Figure S4E). At a later time point, fewer follicles in the ovaries of *Cnot6/6l^{-/-}* mice were positive for the ovulation marker protein prostaglandin synthase 2 (PTGS2) and pentraxin 3 (PTX3), which is downstream of ERK1/2 and $CEBP\alpha/\beta$, than those in the ovaries

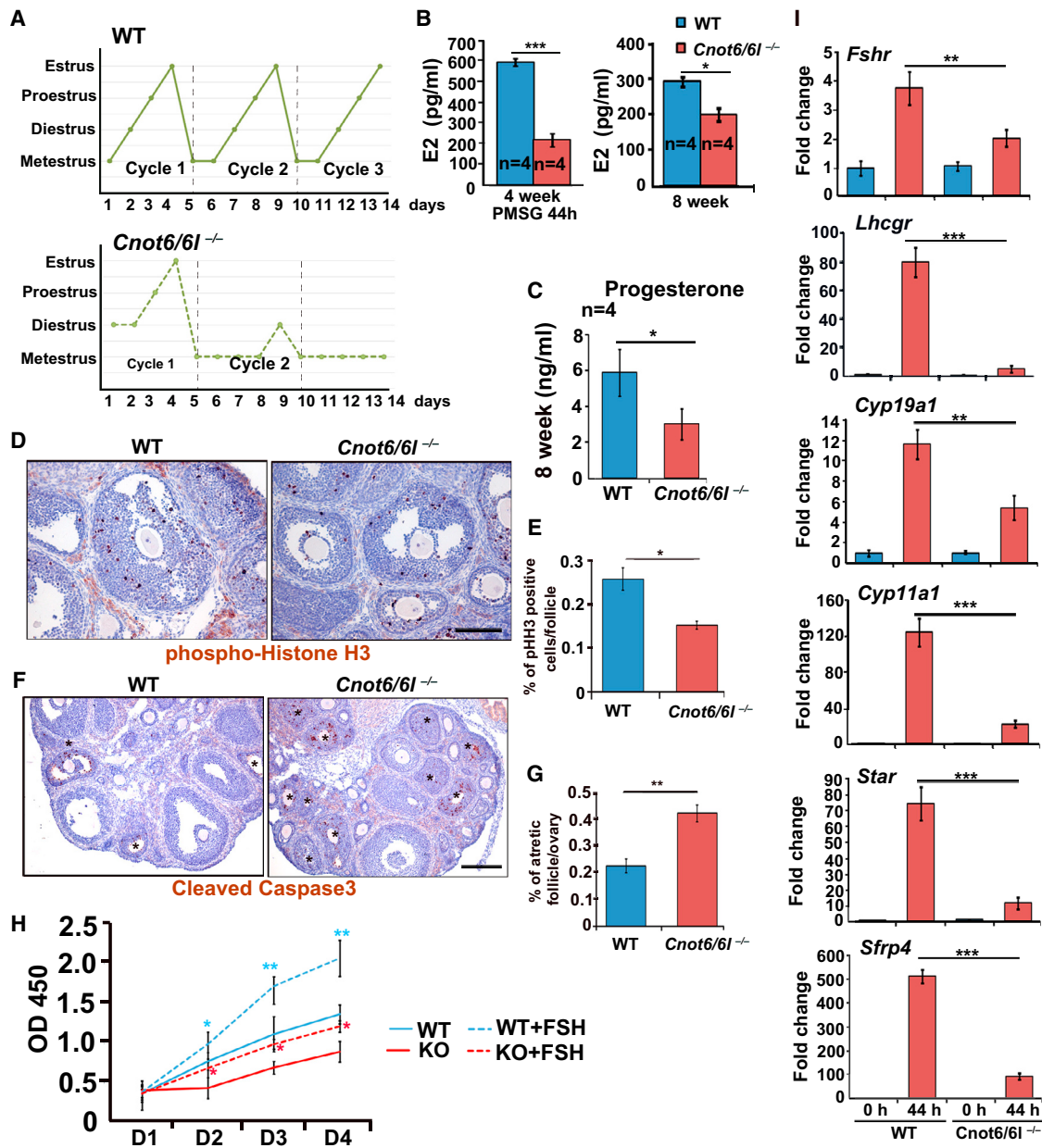


Figure 5. FSH-regulated ovarian functions in WT and *Cnot6/61*^{-/-} female mice

(A) Estrous cycle tests for WT and *Cnot6/61*^{-/-} female mice. The estrous status of mice at 8 weeks (n = 5 for each genotype) was determined through daily cytology examinations of vaginal cell smears.

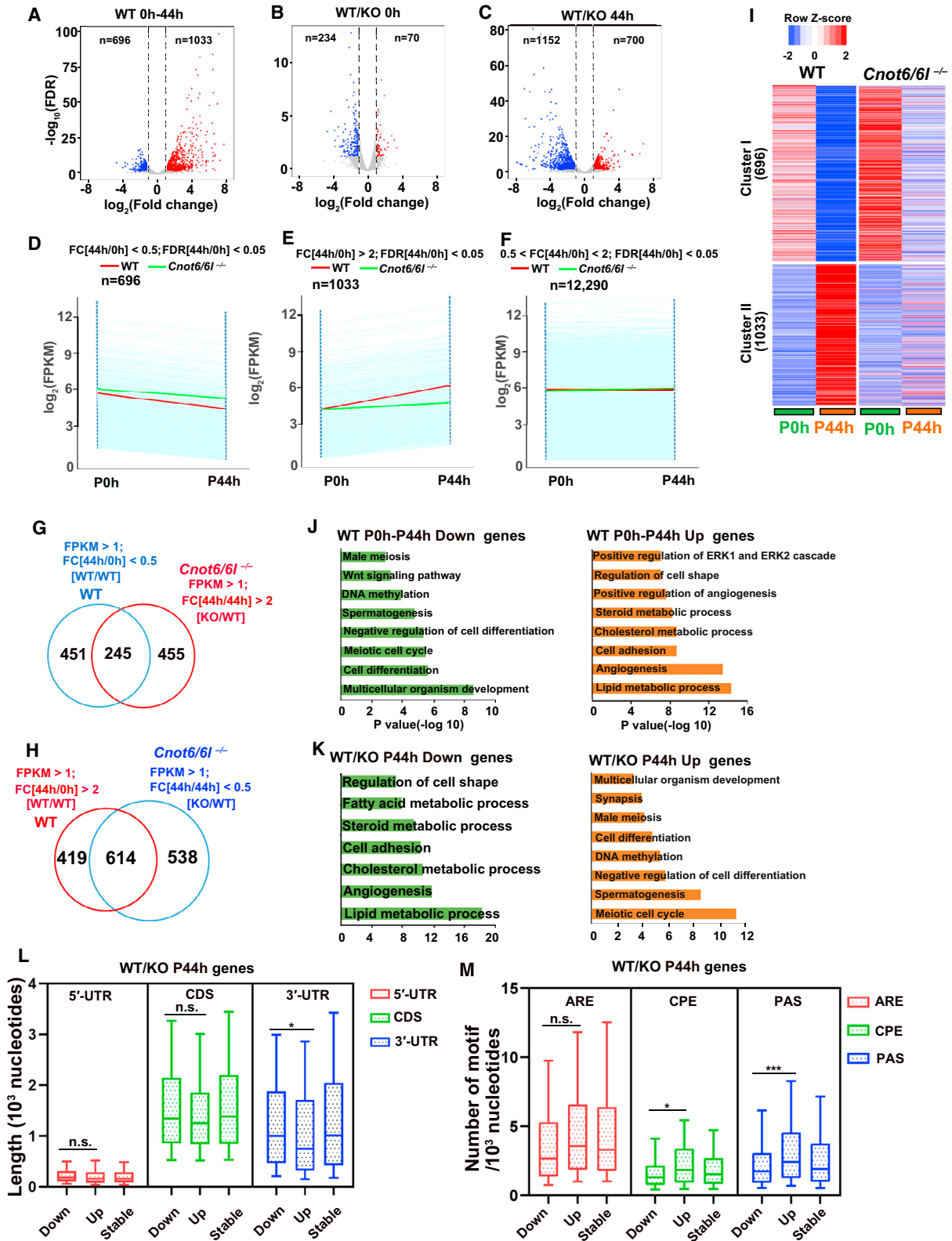
(B and C) Estradiol (B) and progesterone (C) concentrations in serum of WT and *Cnot6/61*^{-/-} female mice. The numbers of mice used are indicated (n). In animals not treated by PMSG, hormone levels were measured at the same stage (diestrus) of the estrous cycle.

(D and E) Immunohistochemistry (D) and quantification results (E) for phospho-histone H3 (pH3-Ser10) in ovaries of 4-week-old WT and *Cnot6/61*^{-/-} female mice at 44 h after PMSG injection. Scale bar, 100 μ m.

(F and G) Immunohistochemistry (F) and quantification results (G) for cleaved caspase 3 in ovaries of 4-week-old WT and *Cnot6/61*^{-/-} female mice 44 h after PMSG injection. Scale bar, 100 μ m. Asterisks indicate atretic follicles.

(H) Cell proliferation determined through optical density at 450 nm (OD₄₅₀). Error bars indicate SEMs. Data are presented as the means \pm SEMs from at least 3 independent experiments, 1-way ANOVA, *p < 0.05, **p < 0.01.

(I) qRT-PCR results showing the relative levels of FSH- and LH-target genes in GCs of 4-week-old WT and *Cnot6/61*^{-/-} female mice 0 and 44 h after PMSG injection. Error bars indicate SEMs. *p < 0.05, **p < 0.01, ***p < 0.001 as determined through 2-tailed Student's t test.



(legend on next page)

of WT mice, as shown through immunofluorescence staining (Figure S4F).

Three epidermal growth factor (EGF)-like paracrine factors (amphiregulin, epiregulin, and β -cellulin) are intrafollicular mediators of LH actions, and are known to be essential for ovulation. The mRNA levels of genes coding for these factors (*Areg*, *Ereg*, and *Btc*) were all lower in granulosa and cumulus cells of *Cnot6/6l*^{-/-} mice after hCG injection (Figure S5A). The LH target genes that are essential for ovarian endocrine functions (*Star* and *Runx2*) and cumulus expansion (*Ptgs2*, *Ptx3*, *Has2*, and *Tnfaip6*) during ovulation had significantly lower expression levels in both GCs and COCs of *Cnot6/6l*^{-/-} mice when compared with those of control mice at 4 h after hCG injection (Figures S5B and S5C). These results suggested that the defective preantral-to-antral follicle transition in response to FSH/PMSG stimulation leads to compromised ovulation in *Cnot6/6l*^{-/-} mice.

FSH triggers mRNA clearance in GCs during preantral-to-antral follicle transition through CNOT6/6L

CNOT6L was reported to mediate maternal mRNA degradation during meiotic maturation in oocytes (Sha et al., 2018). Therefore, we isolated ovarian GCs from mice with or without PMSG treatment (44 h) for RNA sequencing (RNA-seq). Gene expression levels were assessed as fragments per kilobase of transcript per million mapped reads (FPKM). All of the samples were analyzed in duplicate, and all of the replicates showed high correlations (Figure S6A). In the GCs of WT mice, from 0 h (P0) to 44 h (P44) after PMSG treatment (Figure 6A), 1,033 genes were upregulated (fold-change [FC], [P44/P0] > 2) and 696 genes were downregulated (FC [P44/P0] < 0.5).

Next, we compared the gene changes (FPKM > 1) of the GCs in WT and *Cnot6/6l*^{-/-} mice at PMSG 0 and 44 h, respectively. In *Cnot6/6l*^{-/-} animals, the expression levels of many genes were altered. Remarkably, while 70 and 234 genes were respectively upregulated (FC > 2) and downregulated (FC < 0.5) in GCs at P0 (Figure 6B), more genes were upregulated (700) and downregulated (1,152) at P44 (Figure 6C).

We clustered the genes (FPKM > 1) of WT GCs into 3 groups based on their changes from P0 to P44 (Figures 7D–7F). Genes with notable declines in mRNA levels (FC [P44/P0] < 0.5) were identified as cluster I (Figure 6D), those that increased remark-

ably in mRNA levels (FC [P44/P0] > 2) as cluster II (Figure 6E), while the rest were categorized into cluster III (Figure 6F). The transcripts that should be degraded from P0 to P44 accumulated in *Cnot6/6l*^{-/-} GCs (cluster I; Figure 6D). At the same time, the genes whose transcripts should increase from PMSG 0 h to 44 h failed to increase (cluster II; Figure 6E). *Cnot6/6l* had no effect on genes unresponsive to PMSG (cluster III; Figure 6F).

Among the transcripts that apparently accumulated in *Cnot6/6l*^{-/-} GCs (n = 700) from P0 to P44, 245 belonged to cluster I and decreased significantly in WT GCs (Figure 6G). The majority of the gene transcripts that dramatically decreased at P44 (n = 1,152) after *Cnot6/6l* knockout, increased (n = 614) in WT GCs (Figure 6H). The heatmap in Figure 6I showed that the knockout of *Cnot6/6l* caused the accumulation of gene transcripts that normally should have decreased from P0 to P44 and inhibited gene expression that normally should increase during this process.

Gene Ontology (GO) analysis results showed that most of the accumulated transcripts in *Cnot6/6l*^{-/-} GCs (decreased from P0 to P44 in WT GCs) were related to multicellular organism development, cell differentiation, and cell cycle (Figures 6J and 6K). Many of the downregulated transcripts in *Cnot6/6l*^{-/-} GCs (increased from P0 to P44 in WT GCs) were encoded by genes related to metabolism, catalysis, and hormone production (Figures 6J and 6K).

We sought to understand the features of transcripts that apparently accumulated in *Cnot6/6l*^{-/-} GCs at P44. Analysis of the transcripts revealed that the length of the 5' UTR and CDS (coding sequence) were not different in transcripts that were increased at P44. The transcripts increased in *Cnot6/6l* null GCs at P44 had relatively short 3' UTRs (Figure 6L). The 3' UTR contains many types of consensus regulatory sequences for RNA-binding proteins (RBPs). The transcripts that were increased after *Cnot6/6l* knockout had more polyadenylation signals (PASs) and cytoplasmic polyadenylation elements (CPEs) in their 3' UTRs. However, the consensus binding sequence of ZFP36 (AU-rich elements [AREs]) was not enriched in the 3' UTRs of transcripts that were increased in a CNOT6/6l-dependent manner (Figure 6M). Therefore, FSH induced a decrease in a subset of mRNAs in GCs during preantral-to-antral follicle transition. *Cnot6/6l* promoted this process and ensured the hemostasis of GCs.

Figure 6. Genes increased at PMSG 44 h in *Cnot6/6l*^{-/-} GCs

- (A) Volcano map comparing transcripts between WT GCs from PMSG 0 to 44 h. Transcripts decreased or increased >2-fold in *Cnot6/6l*^{-/-} GCs were highlighted with blue or red, respectively.
- (B and C) Volcano map comparing transcripts of WT GCs and *Cnot6/6l*^{-/-} GCs at PMSG 0 h (B) and 44 h (C). Transcripts decreased or increased >2-fold in WT GC samples were highlighted with blue or red, respectively.
- (D–F) Expression pattern of transcripts from PMSG 0 to –44 h. Transcripts with FPKM > 1 were selected. Each light blue line represents the expression level of a single gene, and the center red and green lines represent the median expression level of the cluster in WT and *Cnot6/6l*^{-/-} GCs, respectively.
- (G) Venn diagrams showing the overlap of transcripts that were decreased in WT GCs but increased in *Cnot6/6l*^{-/-} GCs at PMSG 44 h.
- (H) Venn diagrams showing the overlap of transcripts that were increased in WT GCs but decreased in *Cnot6/6l*^{-/-} GCs at PMSG 44 h.
- (I) Heatmap showing transcripts that were significantly increased and decreased during PMSG 0–44 h in WT and *Cnot6/6l*^{-/-} GCs.
- (J) Gene Ontology analysis of transcripts decreased and increased in WT GCs from PMSG 0–44 h.
- (K) Gene Ontology analysis of transcripts decreased and increased in *Cnot6/6l*^{-/-} GCs compared to WT GCs at PMSG 44 h.
- (L) Boxplot of 5' UTR, CDS, and 3' UTR length for decreased, stable, and increased transcripts in *Cnot6/6l*^{-/-} GCs compared to WT GCs at PMSG 44 h. The center value represents the mean length, and the upper and center hinges, the first and third quartiles, respectively.
- (M) Relative numbers of AREs, CPEs, and PASs in the 3' UTR of increased transcripts in *Cnot6/6l*^{-/-} GCs at PMSG 44 h. The value at the center represents the mean length, and the upper and center hinges, the first and third quartiles, respectively.

determined by qPCR. Due to the preference of oligo-dT for long PATs, the ratio of qRT-PCR efficiency between oligo-dT and random primers reflected the PAT length of the detected transcripts (Figure S6B). A significant shortening of PATs was induced by PMSG treatment in WT GCs, but this effect was attenuated in *Cnot6/6l*^{-/-} GCs (Figure S7B).

The *Amh* gene encodes the AMH, which is a crucial factor produced by GCs of growing preantral follicles to repress the overgrowth of their peer follicles (Xu et al., 2018). Immunohistochemical staining of 8-week mouse ovary sections indicated the accumulation of AMH protein after *Cnot6/6l* knockout (Figure S7C). We thus determined PAT length changes of *Amh* transcripts by the PAT assay (Dai et al., 2019). In WT GCs, the PATs of *Amh* transcripts were shortened after PMSG treatment, while no shortening was detected in *Cnot6/6l*^{-/-} GCs (Figure S7D). Quantification of the band shift using ImageJ indicated that the PAT of *Amh* in *Cnot6/6l*^{-/-} GCs was remarkably longer than that in WT GCs after PMSG treatment (Figure S7E). In addition, western blot results showed that AMH protein levels decreased in the GCs of WT mice after PMSG treatment. In contrast, AMH levels were higher in GCs of *Cnot6/6l*^{-/-} mice and did not decrease after PMSG treatment (Figure S7F).

To exclude the effect of transcription activity on the mRNA levels during this process, 50 μM of α-amanitin was used to repress *de novo* gene transcription in cultured GCs. EU (5-ethynyl uridine) staining showed that the transcription activity was dramatically inhibited within 1 h after the α-amanitin treatment (Figure S2D). The addition of FSH to cultured WT GCs accelerated the decrease in *Fos*, *Tex12*, *Amh*, and *Bet3l* transcripts (Figure S7G). However, in *Cnot6/6l*^{-/-} GCs, FSH-induced transcript removal was significantly delayed (Figure S7G). Therefore, during the normal development of GCs, the timely expression of *Cnot6/6l* induced by FSH is at least partially responsible for the deadenylation and degradation of FSH-targeted transcripts.

Potential role of the RBP ZFP36 in mediating CNOT6/6L-dependent mRNA degradation

Studies in mouse oocytes have reported that CNOT6L recruits an adaptor, ZFP36L2, and promotes the degradation of mRNA containing the ARE in the 3' UTR region. Therefore, we also analyzed the expression and localization of ZFP36 family members (ZFP36, ZFP36L1, and ZFP36L2) in mouse ovaries during follicle development by qRT-PCR (Figures 7A and 7B). The amplification efficiency of different PCR primers was normalized so that the expression levels of ZFP36 family members could be compared. The results showed that *Zfp36* and *Zfp36l1*, but not *Zfp36l2*, were expressed in mouse granulosa cells. In addition, the expression level of *Zfp36* was transiently elevated at 24 h after PMSG injection, suggesting that it is a FSH target gene. Western blot and IHC results also showed a transient elevation of ZFP36 protein level after PMSG injection (Figures 7C and 7D). When co-expressed in HeLa cells by plasmid transfection, both CNOT6 and CNOT6L interacted with ZFP36, as determined by a co-immunoprecipitation assay (Figure 7E). To determine the potential role of ZFP36 in the selection of CNOT6/6L substrates, we expressed and immunoprecipitated FLAG-tagged ZFP36 in cultured HeLa cells and

incubated the ZFP36-coated agarose beads with ovarian lysates (Figure 7F). The representative transcripts that displayed CNOT6/6L-dependent decreases after PMSG injection were enriched by ZFP36 in an RNA immunoprecipitation assay. In contrast, the transcripts that are known to accumulate in GCs after PMSG/FSH treatment, including those encoding LH receptor (*Lhcgr*) and aromatase (*Cyp19a1*), as well as *Gapdh*, which is constitutively expressed in most cell types, were not enriched by ZFP36 (Figure 7F). Based on these results, we hypothesized that the FSH-induced mRNAs essential for ovulation are not recruited by ZFP36 to CNOT6/6L; therefore, they can accumulate in antral follicles when the ZFP36-recruited mRNAs are degraded. A paper published during the revision of the present study also reported the expression of ZFP16 in mouse GCs and its key role in triggering destabilization of transcripts encoding natriuretic peptide precursor C (Xi et al., 2021).

DISCUSSION

FSH is indispensable for follicle development beyond the early antral stage (Roy and Albee, 2000; Zhang et al., 2013). FSH stimulates GC proliferation, prevents follicle atresia, and promotes sex hormone synthesis in growing follicles (Ji et al., 2017; Zhou et al., 2017). According to canonical theories, FSH performs these functions by stimulating target gene transcription in GCs. The known FSH target genes include *Ccnd2*, which encodes cyclin D2 and is required for GC proliferation (Han et al., 2013); *Cyp19a1*, which encodes aromatase, the key enzyme of estrogen biosynthesis (Fan et al., 2009; Kidokoro et al., 2009); *Fshr*, which encodes the FSH receptor and endows the GC responsiveness to FSH (Stillely and Segaloff, 2018; Wang and Greenwald, 1993); and *Inhba* and *Inhbb*, which encode activin, a multifunctional growth and differentiation factor of the transforming growth factor-β (TGF-β) family (Reader and Gold, 2015; Vale et al., 1988). Recent studies have revealed previously unnoticed post-transcriptional regulation of ovarian follicle development by gonadotropin.

In this study, we identified *Cnot6* and *Cnot6l* as previously unreported FSH-targeted genes in GCs, which were also required for the efficient formation of antral follicles and ovulation. While FSH induced the transcription of *Cnot6* in GCs through the canonical PI3K-FOXO1 signaling pathway by releasing the transcription-inhibiting factor FOXO1 from the *Cnot6* promoter, FSH stimulated *Cnot6l* expression mainly by activating its mRNA translation. In addition, FSH also downregulated the levels of a subset of existing transcripts in GCs through CNOT6/6L-mediated deadenylation and disability. The latter mechanism appears to be a prompt way to remove the repressing factors for follicle development, such as AMH.

Based on these observations, we propose the hypothesis that FSH supports follicle development at three levels of genetic information flow: (1) transcription of downstream genes, such as *Cyp19a1*, *Fshr*, and *Cnot6*; (2) targeting the 3' UTR of existing transcripts and stimulating mRNA translation (e.g., *Cnot6l*); and (3) destabilizing a subset of existing transcripts through CCR4-NOT-catalyzed PAT shortening. The *in vivo* significance of these mechanisms is demonstrated through the observation

that FSH-dependent follicle developmental events are compromised in the *Cnot6/6l* double-knockout mice.

Limitations of the study

In vitro biochemical evidence suggests that both the CNOT7/8 and the CNOT6/6L subunits are required for the full function of the CCR4-NOT complex in mediating mRNA deadenylation (Mostafa et al., 2020; Sha et al., 2019), whereas the CNOT6 or CNOT6L subunit removes PATs occupied by the cytoplasmic poly(A)-binding proteins (PABPCs), CNOT7, or CNOT8 trims PABPC-free PATs (Kumar and Glaunsinger, 2010; Webster et al., 2018; Yi et al., 2018). However, these working models have not been verified in animals. CCR4-NOT-mediated mRNA deadenylation was described as a housekeeping cellular activity, but the genetic evidence provided by this study showed that mice were viable when both *Cnot6/6l* genes were absent. Considering that CNOT6 and CNOT6L are widely expressed in many somatic cell types, it is unexpected to find that CNOT6/6L are only indispensable in a few *in vivo* biological processes, particularly female reproduction. Our study did not provide an explanation for this apparent discrepancy. Further investigations are required to reveal the redundant mRNA clearance mechanisms *in vivo*. These mechanisms may be either CNOT6/6L independent or CCR4-NOT independent.

It is important to identify key targets of CNOT6/6L that repress the transition of the pre-antral to antral follicle. However, the function of these proposed factors in regulating follicle development cannot be determined by *in vitro* experiments because the survival and proliferation of cultured GCs are not FSH dependent and do not mimic follicle growth *in vivo*. To conclusively indicate the *in vivo* function of these factors, knockout or GC-specific knockout mice need to be generated and their ovarian functions analyzed in future studies. However, the development of pre-antral to antral follicles is a very complex biological process that is regulated by a network of signaling pathways and biological activities. There may not be a specific CNOT6/6L target that can determine, on its own, the transition of pre-antral to antral follicles. More likely, FSH-induced multilayers of transcriptome changes occur, including *de novo* gene transcription (*Cnot6* as a gene identified in this study), translational activation of existing transcripts (e.g., *Cnot6l*), and CNOT6/6L-dependent clearance of a subset of mRNAs. Our RNA-seq results in GCs of WT and *Cnot6/6l* KO mice provided abundant information on these key transcriptome changes during preantral-to-antral follicle transition.

STAR★METHODS

Detailed methods are provided in the online version of this paper and include the following:

- KEY RESOURCES TABLE
- RESOURCE AVAILABILITY
 - Lead contact
 - Materials availability
 - Data and code availability
- EXPERIMENTAL MODEL AND SUBJECT DETAILS

- Animals
- Granulosa cell
- METHOD DETAILS
 - Fertility test
 - Superovulation
 - Histological analysis and immunohistochemistry (IHC)
 - Immunofluorescence
 - Hormone level tests
 - Western blot analysis
 - Plasmid transfection and Foxo1 RNA interference
 - Chromatin immunoprecipitation (ChIP)
 - Cell culture, plasmid transfection, and ribonucleoprotein immunoprecipitation (RIP) assay
 - Evaluation of the proliferation of granulosa cells
 - 5-ethynyl uridine (EU) incorporation assay
 - Poly(A) tail (PAT) assay
 - RNA isolation and library construction
 - RNA isolation, reverse transcription, and quantitative PCR
- QUANTIFICATION AND STATISTICAL ANALYSIS
 - RNA-seq data analysis
 - Statistical analysis

SUPPLEMENTAL INFORMATION

Supplemental information can be found online at <https://doi.org/10.1016/j.celrep.2021.110007>.

ACKNOWLEDGMENTS

This study is supported by the National Natural Science Foundation of China (31930031 and 31890781 to H.Y.-F.), the China Postdoctoral Science Foundation (2021M692824 and 2021T140603 to X.-X.D.), the National Key Research and Developmental Program of China (SQ2020YFF0426502 to Q.-Q.S.), and the Key Research and Development Program of Zhejiang Province (2021C03098 and 2021C03100).

AUTHOR CONTRIBUTIONS

H.-Y.F. conceived the project. H.-Y.F., X.-X.D., and Z.-Y.J. designed and analyzed the experiments. X.-X.D., Z.-Y.J., Y.-W.W., Q.-Q.S., Y.L., J.-Y.D., and W.-D.X. performed the experiments. X.-X.D. and H.-Y.F. wrote the paper.

DECLARATION OF INTERESTS

The authors declare no competing interests.

Received: November 24, 2020

Revised: July 27, 2021

Accepted: October 26, 2021

Published: November 16, 2021

REFERENCES

- Aslam, A., Mittal, S., Koch, F., Andrau, J.-C., and Winkler, G.S. (2009). The Ccr4-NOT deadenylase subunits CNOT7 and CNOT8 have overlapping roles and modulate cell proliferation. *Mol. Biol. Cell* 20, 3840–3850.
- Berthet, C., Morera, A.-M., Asensio, M.-J., Chauvin, M.-A., Morel, A.-P., Djoud, F., Magaud, J.-P., Durand, P., and Rouault, J.-P. (2004). CCR4-associated factor CAF1 is an essential factor for spermatogenesis. *Mol. Cell. Biol.* 24, 5808–5820.

- Brind'Amour, J., Liu, S., Hudson, M., Chen, C., Karimi, M.M., and Lorincz, M.C. (2015). An ultra-low-input native ChIP-seq protocol for genome-wide profiling of rare cell populations. *Nat. Commun.* **6**, 6033.
- Dai, X.X., Jiang, J.C., Sha, Q.Q., Jiang, Y., Ou, X.H., and Fan, H.Y. (2019). A combinatorial code for mRNA 3'-UTR-mediated translational control in the mouse oocyte. *Nucleic Acids Res.* **47**, 328–340.
- Doidge, R., Mittal, S., Aslam, A., and Winkler, G.S. (2012). Deadenylation of cytoplasmic mRNA by the mammalian Ccr4-Not complex. *Biochem. Soc. Trans.* **40**, 896–901.
- Fan, H.Y., Liu, Z., Cahill, N., and Richards, J.S. (2008). Targeted disruption of Pten in ovarian granulosa cells enhances ovulation and extends the life span of luteal cells. *Mol. Endocrinol.* **22**, 2128–2140.
- Fan, H.Y., Liu, Z., Shimada, M., Sterneck, E., Johnson, P.F., Hedrick, S.M., and Richards, J.S. (2009). MAPK3/1 (ERK1/2) in ovarian granulosa cells are essential for female fertility. *Science* **324**, 938–941.
- Fan, H.Y., O'Connor, A., Shitanaka, M., Shimada, M., Liu, Z., and Richards, J.S. (2010). Beta-catenin (CTNNB1) promotes preovulatory follicular development but represses LH-mediated ovulation and luteinization. *Mol. Endocrinol.* **24**, 1529–1542.
- Fan, H.Y., Liu, Z., Johnson, P.F., and Richards, J.S. (2011). CCAAT/enhancer-binding proteins (C/EBP)- α and - β are essential for ovulation, luteinization, and the expression of key target genes. *Mol. Endocrinol.* **25**, 253–268.
- Flyamer, I.M., Gassler, J., Imakaev, M., Brandão, H.B., Ulianov, S.V., Abdennur, N., Razin, S.V., Mirny, L.A., and Tachibana-Konwalski, K. (2017). Single-nucleus Hi-C reveals unique chromatin reorganization at oocyte-to-zygote transition. *Nature* **544**, 110–114.
- Gou, L.-T., Dai, P., Yang, J.-H., Xue, Y., Hu, Y.-P., Zhou, Y., Kang, J.-Y., Wang, X., Li, H., Hua, M.-M., et al. (2014). Pachytene piRNAs instruct massive mRNA elimination during late spermiogenesis. *Cell Res.* **24**, 680–700.
- Han, Y., Xia, G., and Tsang, B.K. (2013). Regulation of cyclin D2 expression and degradation by follicle-stimulating hormone during rat granulosa cell proliferation in vitro. *Biol. Reprod.* **88**, 57.
- Horvat, F., Fulka, H., Jankele, R., Malik, R., Jun, M., Solcova, K., Sedlacek, R., Vlahovick, K., Schultz, R.M., and Svoboda, P. (2018). Role of *Cnot6l* in maternal mRNA turnover. *Life Sci. Alliance* **1**, e201800084.
- Hosseini, G., Khanmohammadi, M., Sahranavard Fard, P., Heidarian, Y., Kazemnejad, S., and Akhondi, M.M. (2016). Exogenous Secreted Frizzled-Related Protein-4 Modulates Steroidogenesis of Rat Granulosa Cells through Wnt/ β -catenin and PI3K/AKT Signaling Pathways. *Avicenna J. Med. Biotechnol.* **8**, 159–168.
- Hsieh, M., Mulders, S.M., Friis, R.R., Dharmarajan, A., and Richards, J.S. (2003). Expression and localization of secreted frizzled-related protein-4 in the rodent ovary: evidence for selective up-regulation in luteinized granulosa cells. *Endocrinology* **144**, 4597–4606.
- Ji, S.Y., Liu, X.M., Li, B.T., Zhang, Y.L., Liu, H.B., Zhang, Y.C., Chen, Z.J., Liu, J., and Fan, H.Y. (2017). The polycystic ovary syndrome-associated gene *Yap1* is regulated by gonadotropins and sex steroid hormones in hyperandrogenism-induced oligo-ovulation in mouse. *Mol. Hum. Reprod.* **23**, 698–707.
- Kidokoro, K., Ino, K., Hirose, K., Kajiyama, H., Hosono, S., Suzuki, T., Kawase, T., Hiraki, A., Hamajima, N., Tanaka, H., et al. (2009). Association between CYP19A1 polymorphisms and sex hormones in postmenopausal Japanese women. *J. Hum. Genet.* **54**, 78–85.
- Kumar, G.R., and Glaunsinger, B.A. (2010). Nuclear import of cytoplasmic poly(A) binding protein restricts gene expression via hyperadenylation and nuclear retention of mRNA. *Mol. Cell Biol.* **30**, 4996–5008.
- Liu, Z., Castrillon, D.H., Zhou, W., and Richards, J.S. (2013). FOXO1/3 depletion in granulosa cells alters follicle growth, death and regulation of pituitary FSH. *Mol. Endocrinol.* **27**, 238–252.
- Liu, Z., Ren, Y.A., Pangas, S.A., Adams, J., Zhou, W., Castrillon, D.H., Wilhelm, D., and Richards, J.S. (2015). FOXO1/3 and PTEN Depletion in Granulosa Cells Promotes Ovarian Granulosa Cell Tumor Development. *Mol. Endocrinol.* **29**, 1006–1024.
- Manna, P.R., Stetson, C.L., Slominski, A.T., and Pruitt, K. (2016). Role of the steroidogenic acute regulatory protein in health and disease. *Endocrine* **51**, 7–21.
- Maryati, M., Kaur, I., Jadhav, G.P., Olotu-Umoren, L., Oveh, B., Hashmi, L., Fischer, P.M., and Winkler, G.S. (2014). A fluorescence-based assay suitable for quantitative analysis of deadenylase enzyme activity. *Nucleic Acids Res.* **42**, e30.
- Mostafa, D., Takahashi, A., Yanagiya, A., Yamaguchi, T., Abe, T., Kureha, T., Kuba, K., Kanegae, Y., Furuta, Y., Yamamoto, T., and Suzuki, T. (2020). Essential functions of the CNOT7/8 catalytic subunits of the CCR4-NOT complex in mRNA regulation and cell viability. *RNA Biol.* **17**, 403–416.
- Parakh, T.N., Hernandez, J.A., Grammer, J.C., Weck, J., Hunzicker-Dunn, M., Zeleznik, A.J., and Nilson, J.H. (2006). Follicle-stimulating hormone/cAMP regulation of aromatase gene expression requires beta-catenin. *Proc. Natl. Acad. Sci. USA* **103**, 12435–12440.
- Reader, K.L., and Gold, E. (2015). Activins and activin antagonists in the human ovary and ovarian cancer. *Mol. Cell. Endocrinol.* **415**, 126–132.
- Robinson, M.D., McCarthy, D.J., and Smyth, G.K. (2010). edgeR: a Bioconductor package for differential expression analysis of digital gene expression data. *Bioinformatics* **26**, 139–140.
- Roy, S.K., and Albee, L. (2000). Requirement for follicle-stimulating hormone action in the formation of primordial follicles during perinatal ovarian development in the hamster. *Endocrinology* **141**, 4449–4456.
- Schneider, C.A., Rasband, W.S., and Eliceiri, K.W. (2012). NIH Image to ImageJ: 25 years of image analysis. *Nat. Methods* **9**, 671–675.
- Sha, Q.-Q., Yu, J.-L., Guo, J.-X., Dai, X.-X., Jiang, J.-C., Zhang, Y.-L., Yu, C., Ji, S.-Y., Jiang, Y., Zhang, S.-Y., et al. (2018). CNOT6L couples the selective degradation of maternal transcripts to meiotic cell cycle progression in mouse oocyte. *EMBO J.* **37**, e99333.
- Sha, Q.Q., Zhang, J., and Fan, H.Y. (2019). A story of birth and death: mRNA translation and clearance at the onset of maternal-to-zygotic transition in mammals. *Biol. Reprod.* **101**, 579–590.
- Stille, J.A.W., and Segaloff, D.L. (2018). FSH Actions and Pregnancy: Looking Beyond Ovarian FSH Receptors. *Endocrinology* **159**, 4033–4042.
- Sun, X., Su, Y., He, Y., Zhang, J., Liu, W., Zhang, H., Hou, Z., Liu, J., and Li, J. (2015). New strategy for in vitro activation of primordial follicles with mTOR and PI3K stimulators. *Cell Cycle* **14**, 721–731.
- Temme, C., Simonelig, M., and Wahle, E. (2014). Deadenylation of mRNA by the CCR4-NOT complex in *Drosophila*: molecular and developmental aspects. *Front. Genet.* **5**, 143.
- Vale, W., Rivier, C., Hsueh, A., Campen, C., Meunier, H., Bicsak, T., Vaughan, J., Corrigan, A., Bardin, W., Sawchenko, P., et al. (1988). Chemical and biological characterization of the inhibin family of protein hormones. *Recent Prog. Horm. Res.* **44**, 1–34.
- Wang, X.N., and Greenwald, G.S. (1993). Synergistic effects of steroids with FSH on folliculogenesis, steroidogenesis and FSH- and hCG-receptors in hypophysectomized mice. *J. Reprod. Fertil.* **99**, 403–413.
- Webster, M.W., Chen, Y.H., Stowell, J.A.W., Alhusaini, N., Sweet, T., Graveley, B.R., Collier, J., and Passmore, L.A. (2018). mRNA Deadenylation Is Coupled to Translation Rates by the Differential Activities of Ccr4-Not Nucleases. *Mol. Cell* **70**, 1089–1100.e8.
- Wiederhold, K., and Passmore, L.A. (2010). Cytoplasmic deadenylation: regulation of mRNA fate. *Biochem. Soc. Trans.* **38**, 1531–1536.
- Winkler, G.S., and Balacco, D.L. (2013). Heterogeneity and complexity within the nuclease module of the Ccr4-Not complex. *Front. Genet.* **4**, 296.
- Xi, G., An, L., Wang, W., Hao, J., Yang, Q., Ma, L., Lu, J., Wang, Y., Wang, W., Zhao, W., et al. (2021). The mRNA-destabilizing protein Tristetraprolin targets “meiosis arrester” *Nppc* mRNA in mammalian preovulatory follicles. *Proc. Natl. Acad. Sci. USA* **118**, e2018345118.
- Xu, J., Xu, F., Lawson, M.S., Tkachenko, O.Y., Ting, A.Y., Kahl, C.A., Park, B.S., Stouffer, R.R., and Bishop, C.V. (2018). Anti-Müllerian hormone is a survival factor and promotes the growth of rhesus macaque preantral follicles during matrix-free culture. *Biol. Reprod.* **98**, 197–207.

Yi, H., Park, J., Ha, M., Lim, J., Chang, H., and Kim, V.N. (2018). PABP Cooperates with the CCR4-NOT Complex to Promote mRNA Deadenylation and Block Precocious Decay. *Mol. Cell* 70, 1081–1088.e5.

Yu, C., Ji, S.Y., Sha, Q.Q., Dang, Y., Zhou, J.J., Zhang, Y.L., Liu, Y., Wang, Z.W., Hu, B., Sun, Q.Y., et al. (2016). BTG4 is a meiotic cell cycle-coupled maternal-zygotic-transition licensing factor in oocytes. *Nat. Struct. Mol. Biol.* 23, 387–394.

Zhang, Y.L., Yu, C., Ji, S.Y., Li, X.M., Zhang, Y.P., Zhang, D., Zhou, D., and Fan, H.Y. (2013). TOP2 β is essential for ovarian follicles that are hypersensitive to chemotherapeutic drugs. *Mol. Endocrinol.* 27, 1678–1691.

Zhou, J., Yao, W., Li, C., Wu, W., Li, Q., and Liu, H. (2017). Administration of follicle-stimulating hormone induces autophagy via upregulation of HIF-1 α in mouse granulosa cells. *Cell Death Dis.* 8, e3001.

STAR★METHODS

KEY RESOURCES TABLE

REAGENT or RESOURCE	SOURCE	IDENTIFIER
Antibodies		
Rabbit polyclonal anti-CNOT6/6L	Abcam	Cat# ab86209; RRID: AB_1924895
Rabbit polyclonal anti-CNOT7	Abcam	Cat# ab195587; RRID: AB_2801659
Rabbit polyclonal anti-pERK1/2	Cell Signaling Technology	Cat# 9101; RRID: AB_331646
Rabbit polyclonal anti-FOXO1	Cell Signaling Technology	Cat# 2880S; RRID: AB_2106495
Rabbit polyclonal anti-DDB1	Epitomics	Cat# 3821-1; RRID: AB_10896720
Rabbit polyclonal anti-pH3S10	Cell Signaling Technology	Cat# 9701S; RRID: AB_331535
Rabbit polyclonal anti-Cleaved Caspase 3	Cell Signaling Technology	Cat# 9669; RRID: AB_2069869
Rabbit polyclonal anti-pAKT	Cell Signaling Technology	Cat# 3787S; RRID: AB_331170
Rabbit polyclonal anti-PTGS2	Santa Cruz Biotechnology	Cat# sc-1747; RRID: AB_2084976
Mouse monoclonal anti-FLAG	Sigma-Aldrich	Cat# F3165; RRID: AB_259529
Rabbit polyclonal anti-AKT	Cell Signaling Technology	Cat# 9272; RRID: AB_329827
Rabbit polyclonal anti-ZFP36	Proteintech	Cat# 12737-1-AP; RRID: AB_10598485
Biological samples		
Healthy WT C57BL/6J mice ovary tissue	Jackson Laboratory	Cat# 5657312, RRID: MGI: 5657312
<i>Cnot6/6l^{-/-}</i> C57BL/6J mice ovary tissue	This paper	N/A
<i>Cnot6^{-/-}</i> C57BL/6J mice ovary tissue	This paper	N/A
Chemicals, peptides, and recombinant proteins		
PMSG	Ningbo Sansheng Pharmaceutical Co.,Ltd	Cat# 110914564
Rabbit IgG	Millipore	Cat# NI01
LY294002	MedChem Express	Cat# 154447-36-6
α -Amanitin	Absin	Cat# 23109-05-9
740Y-P	MedChem Express	Cat# 1236188-16-1
Fetal bovine serum (FBS)	Sigma-Aldrich	Cat# F4135
Dulbecco's Modified Eagle Medium (DMEM)	GIBCO	Cat# 11960-04
Critical commercial assays		
RNeasy Mini kit	QIAGEN	Cat# 74106
Power SYBR Green PCR Master Mix	Life Technologies	Cat# 4367659
Vectastain ABC kit	Vector Laboratories	Cat# PK-6100
DAB Substrate Kit	Vector Laboratories	Cat# SK-4100
Lipofectamine 2000	Invitrogen	Cat# 11668-027
Lipofectamine RNAiMAX	Invitrogen	Cat# 13778-150
Chromatin IP kit	Cell Signaling Technology	Cat# 9003
Cell Counting Kit-8	MedChem Express	Cat# HY-K0301
Click-iT® RNA Alexa Fluor® 488 Imaging Kit	Thermo Fisher Scientific	Cat# C10329
Deposited data		
Raw and analyzed data	This paper	GEO: GSE158773
Experimental models: cell lines		
Granulosa cells	This paper	N/A
Experimental models: organisms/strains		
Mouse: <i>Cnot6^{-/-}</i> : C57BL/6J	The Fan Laboratory	N/A
Mouse: <i>Cnot6l^{-/-}</i> : C57BL/6J	The Fan Laboratory	N/A

(Continued on next page)

Continued

REAGENT or RESOURCE	SOURCE	IDENTIFIER
Mouse: <i>Cnot6/6l^{-/-}</i> : C57BL/6J	The Fan Laboratory	N/A
Mouse: WT: C57BL/6J	Jackson Laboratory	Cat# 5657312, RRID: MGI: 5657312
Oligonucleotides		
Pat assay targeting sequence: <i>Amh</i> -pat-F: 5'-TACGCGGGCAAGCTGCTCAT-3'	This paper	N/A
Pat assay targeting sequence: <i>Amh</i> -pat-R: 5'-GCGAGCTCCGCGCCGCGTTTTTTTT-3'	This paper	N/A
Primers for Real-time PCR, see Table S3	This paper	N/A
Recombinant DNA		
<i>mCherry</i> -3'-UTR _{SV40}	This paper	N/A
Flag- <i>Gfp</i> -3'-UTR _{<i>Cnot6l</i>}	This paper	N/A
Flag-ZFP36	This paper	N/A
Flag	This paper	N/A
Software and algorithms		
ImageJ	Schneider et al., 2012 (Schneider et al., 2012)	https://imagej.nih.gov/ij/
GraphPad Prism 8.3.0	GraphPad	https://www.graphpad.com/
Tophat	Center for Bioinformatics and Computational Biology	http://tophat.cbcb.umd.edu/
Cufflinks	Center for Bioinformatics and Computational Biology	http://cufflinks.cbcb.umd.edu
ZEN	ZEISS	https://www.zeiss.com/microscopy/us/products/microscope-software/zen.html

RESOURCE AVAILABILITY

Lead contact

All requests for further information or requests for resources and reagents should be directed to the Lead Contact, Heng-Yu Fan (hyfan@zju.edu.cn).

Materials availability

Please direct resource and reagent requests to the Lead Contact specified above, Heng-Yu Fan.

Data and code availability

- RNA-seq data were deposited in the NCBI Gene Expression Omnibus database under the accession code GSE158773. To review GEO accession GSE158773: Go to <https://www.ncbi.nlm.nih.gov/geo/query/acc.cgi?acc=GSE158773>. Enter token wvkjgicavxkpczj into the box.
- This paper does not report original code.
- Any additional information required to reanalyze the data reported in this paper is available from the lead contact upon request.

EXPERIMENTAL MODEL AND SUBJECT DETAILS

Animals

All mouse strains had a C57B6 background. *Cnot6l^{-/-}* mice have been previously reported. *Cnot6l^{-/-}* mice were generated using the CRISPR-CAS9 system, as shown in Figure S1a of another manuscript under review. Founder mice were identified by genotyping PCR and crossed with wild-type C57B6 partners to ensure germline transmission and to avoid any potential off-targeting effects. Mice were bred under SPF conditions at 20–22°C, with a 12/12 h light/dark cycle, 50%–70% humidity, and food and water provided *ad libitum*. Animals were treated according to the guidelines of the Zhejiang University Animal Research Committee.

4-week-old female mice were used to collect granulosa cells. We detected the ovarian morphology of WT and *Cnot6/6l^{-/-}* female mice at 4 weeks, 8 weeks, and 6 months.

Granulosa cell

Granulosa cells were harvested from PMSG-primed (24 h) PD23 female mice. Granulosa cells were released from antral follicles by puncturing with a 26.5-gauge needle under a stereoscope. Cells were cultured at a density of 1×10^6 cells in Dulbecco's modified Eagle's Medium/F12 medium (GIBCO) containing 5% fetal bovine serum (Sigma-Aldrich), 100 U/mL penicillin, and 100 mg/mL streptomycin in 24-well culture dishes. After overnight culture, cells were washed and cultured in serum-free medium before any further treatment. To induce the expression of FSH target genes *in vitro*, granulosa cells were treated with 100 ng/mL recombinant FSH (Sigma) for 12–24 h.

METHOD DETAILS

Fertility test

Eight-week-old female mice ($n = 6$ for each genotype) were continuously mated with 10- to 12-week-old fertile males over 40 weeks. The number of pups and litters was recorded, and fertility rates were determined.

Superovulation

Female mice (21–23 days old) were intraperitoneally injected with 5 IU of PMSG (Ningbo Sansheng Pharmaceutical Co., Ltd., P. R. China). After 44 h, mice were injected with 5 IU of hCG (Ningbo Sansheng Pharmaceutical Co., Ltd., P. R. China). Oocyte/cumulus masses were surgically removed from the oviducts 16 hours later and the numbers of oocytes were counted after digestion with 0.3% hyaluronidase (Sigma-Aldrich).

Histological analysis and immunohistochemistry (IHC)

Ovaries were fixed overnight in 10% PBS buffered formalin and then embedded in paraffin. Ovary samples were serially sectioned at 5 μ m thickness and stained with hematoxylin and eosin. The number of follicles was determined by recording the number of oocyte nuclei in all sections. These criteria were used to determine the follicle stages: primordial follicles, small oocytes surrounded by a single layer of flat granulosa cells; primary follicles, middle-sized oocytes surrounded by a single layer of cubical granulosa cells; early secondary follicles, containing a middle-sized oocyte surrounded by 2–3 layer of cubical granulosa cells; late secondary follicles, containing a large oocyte surrounded by more than three layers of granulosa cells but have no follicle antrum; and antral follicles, presence of a follicle cavity.

For IHC, sections were deparaffinized, rehydrated, and incubated with primary antibodies (Table S2) for 1 h at 25°C, followed by biotin-labeled secondary antibodies for 30 min. The staining procedure was performed using the Vectastain ABC kit and DAB peroxidase substrate kit (Vector Laboratories, Burlingame, CA, USA).

Immunofluorescence

Primary granulosa cells were seeded on coverslips. Twenty-four hours later, cells were washed with PBS, fixed with 4% paraformaldehyde, permeabilized with PBS containing 0.3% Triton X-100 (PBST), and incubated with blocking buffer (PBST containing 5% bovine serum albumin). Cells were sequentially probed with primary antibodies and Alexa Fluor 594- or 488-conjugated secondary antibodies. Slides were mounted using VectaShield with 4',6-diamidino-2-phenylindole (DAPI, Vector Laboratories). Digital images were acquired using an epifluorescence microscope (Nikon Eclipse80i) with 20–100x objectives.

Hormone level tests

Mice were anesthetized and blood was collected by cardiac puncture. Serum and blood cells were separated by centrifugation. Serum hormone levels were determined by Di'an Medical Diagnostics Limited Corporation (Hangzhou, China).

Western blot analysis

Granulosa cells were lysed with SDS sample buffer and heated for 5 min at 95°C. Protein lysates (30 μ g total protein per lane) were separated through SDS-PAGE and electrophoretically transferred to PVDF membranes (Millipore Corp., Bedford, MA, USA), followed by blocking in TBST containing 5% skim milk (BD, Franklin Lakes, NJ, USA) for 30 min. After probing with primary antibodies, the membranes were washed in TBST, incubated with an HRP-linked secondary antibody (Jackson ImmunoResearch Laboratories) for 1 h, followed by three washes with TBST. Bound antibodies were detected using the Super Signal West Femto maximum sensitivity substrate (Thermo Fisher Scientific Inc., Waltham, MA, USA). The primary antibodies and dilution factors used are listed in Table S5.

Plasmid transfection and Foxo1 RNA interference

The *mCherry-3'-UTR_{SV40}* and *Flag-Gfp-3'-UTR_{Cnot6l}* plasmids were co-transfected into granulosa cells with Lipofectamine 2000 (Invitrogen, 0.5 μ g of each plasmid per well of a 24-well plate). After transfection, cells were treated with FSH and LY294002 for 24 h. The expression of mCherry and FLAG-GFP was detected through fluorescence and western blotting.

Transient siRNA (*siControl* and *siFoxo1*) transfection was performed in cultured primary granulosa cells using Lipofectamine RNAi-MAX (Invitrogen, 50 nmol siRNAs per well of a 24-well plate). After 48 h of transfection, cells were lysed for RNA isolation or western blot analysis.

Chromatin immunoprecipitation (ChIP)

The ChIP assay was performed using a simple ChIP Enzymatic Chromatin IP kit (Cell Signaling) according to the manufacturer's protocol. One microgram of rabbit IgG (PP6421-K; Millipore) or FOXO1 antibody (Cell Signaling; 2880S) was used in each immunoprecipitation reaction. Ten percent of the cell lysate from each sample was obtained before immunoprecipitation and used as input. The input and immunoprecipitated DNA fragments were purified and subjected to RT-qPCR. The PCR primer sequences used are listed in Table S3.

Cell culture, plasmid transfection, and ribonucleoprotein immunoprecipitation (RIP) assay

Cells were cultured in Dulbecco's Modified Eagle Medium containing 10% fetal bovine serum and 1% penicillin–streptomycin solution (GIBCO) in a humidified incubator containing 5% CO₂ at 37°C. Plasmids were transfected by using Lipofectamine 2000 (Invitrogen). After the transfection for 48 h, the cells were lysed in lysis buffer (50 mM Tris–HCl [pH 7.4], 1% Triton X-100, 150 mM NaCl, 5 mM ethylenediaminetetraacetic acid (EDTA), protease inhibitor cocktail and RNase inhibitor). After centrifugation, the supernatant was immunoprecipitated with the designated antibody (Sigma) in the ovarian lysate. After incubation for 4 hours at 4°C, beads were thoroughly washed with washing buffer (50 mM Tris–HCl [pH 7.4], 0.1% Triton X-100, 500 mM NaCl, 5 mM EDTA, protease inhibitor cocktail and RNase inhibitor). According to the manufacturer's instructions, the RNA bound to the beads was extracted using the RNeasy Mini kit (QIAGEN, 74106), and were reverse-transcribed with Moloney Murine Leukemia Virus (M - MLV) (Invitrogen). The relative abundance of cDNA was analyzed through quantitative polymerase chain reaction (qPCR).

Evaluation of the proliferation of granulosa cells

Proliferation of granulosa cells was evaluated using the Cell Counting Kit-8 (CCK-8; MedChem Express) according to the manufacturer's protocol. In brief, cells were seeded into each well of a 96-well plate and cultured with 100 μ L DMEM and 2% FBS for 1–5 days. At the specified time, 10 μ L CCK-8 was added to each well, and the cells were further incubated for 4 h. After incubation, the optical density at 450 nm (OD450) was determined using a microplate reader.

5-ethynyl uridine (EU) incorporation assay

Granulosa cells were cultured in DMEM with 50 μ M 5-ethynyl uridine (EU) for 2 h. Fixation, permeabilization, and staining were performed according to the manufacturer's protocol using the Click-iT[®] RNA Alexa Fluor[®] 488 Imaging Kit (Thermo Fisher Scientific). Granulosa cell imaging was performed using an epifluorescence microscope (Nikon Eclipse80i) with 20–100x objectives.

Poly(A) tail (PAT) assay

Total RNA was isolated from oocytes at the indicated stages using the RNeasy Mini kit (QIAGEN). The RNA was hybridized with or without oligodT(20) before RNaseH treatment. RNA was purified and polymerized with 5 mM GTP and ITP in RNase-free water for 1 h at 37°C using poly(A) polymerase (Affymetrix). Reverse transcription was performed using the SuperScript III kit (Invitrogen) with C10T2 DNA primer (5'-CCCCCCCCCTT-3'). The products were subjected to PCR with gene-specific primers (Table S3) and PAT2 (5'-CAGGA AACAGCTATGAC CCCCCCCCCCTT 3') under the following conditions: 30 s at 94°C, 60 s at 56°C, and 60 s at 72°C. PCR products were analyzed on a 2.5% agarose gel.

RNA isolation and library construction

Granulosa cells were collected from WT and *Cnot6/6l^{-/-}* mice before and after PMSG injections (44 h). Total RNA was extracted from each sample using the RNeasy Mini kit (QIAGEN) according to the manufacturer's protocol. Our library construction is based on previously reported methods (Flyamer et al., 2017). Detect the quality of cDNA library by Q-SEP using Standard S2 cartridge. TruePrepR DNA Library Prep Kit V2 was used to cut 0.5 ng cDNA into approximately 300 bp fragments, and VAHTS DNA Clean beads were used to capture the cDNA and construct the RNA-seq library. The sequencing depth is 30 million reads per sample.

RNA isolation, reverse transcription, and quantitative PCR

Total RNA was extracted using the RNeasy Mini kit (QIAGEN) according to the manufacturer's instructions, and was reverse-transcribed using random primers except for the experiments mentioned in Figure S7B. In the experiments described in Figure S7B, each RNA sample was split into two samples and reverse-transcribed using random primers oligo-(dT) or random primers, respectively. Quantitative PCR (qPCR) analysis was performed using Power SYBR Green PCR Master Mix (Applied Biosystems, Life Technologies) and the Applied Biosystems 7500 Real-Time PCR System. Relative mRNA levels were calculated normalizing the levels of endogenous β -actin mRNA (internal control). The relative transcript levels of samples were compared to the control, and the fold-changes were calculated. For each experiment, qPCR was performed in triplicates. Primer sequences are listed in Table S3.

QUANTIFICATION AND STATISTICAL ANALYSIS

RNA-seq data analysis

We aligned RNA-seq reads sequenced through IlluminaHiSeq 2500 to *Mus musculus* UCSC mm9 references with the Tophat software (<http://tophat.cbcb.umd.edu/>), and calculated the FPKM of each gene using Cufflinks (<http://cufflinks.cbcb.umd.edu/>). We

analyzed the transcripts in the original data using edgeR (Robinson et al., 2010). The information on false discovery rate (FDR) is added to the supplemental datasets. Differentially expressed genes were assessed using edgeR at a P -value of < 0.05 , and FC of > 2 or < 0.5 . GO analysis for enrichment of DEGs was performed using the Database for Annotation, Visualization, and Integrated Discovery (DAVID).

Statistical analysis

Results are presented as means \pm SEM. Each experiment included at least three independent samples and was repeated at least three times. Results from two experimental groups were compared using two-tailed unpaired Student's t tests. Statistically significant values of $p < 0.05$, $p < 0.01$, and $p < 0.001$ are indicated by asterisks (*), (**), and (***), respectively. We used ANOVA to determine statistical differences in experiments with more than two treatment groups. Data are presented as the mean \pm SEM from at least three independent experiments, one-way ANOVA, * $p < 0.05$, ** $p < 0.01$. n.s.: nonsignificant.

Cell Reports, Volume 37

Supplemental information

**CNOT6/6L-mediated mRNA degradation in ovarian
granulosa cells is a key mechanism
of gonadotropin-triggered follicle development**

Xing-Xing Dai, Zhi-Yan Jiang, Yun-Wen Wu, Qian-Qian Sha, Yang Liu, Jia-Yi Ding, Wen-Dong Xi, Jing Li, and Heng-Yu Fan

Supplementary Figures

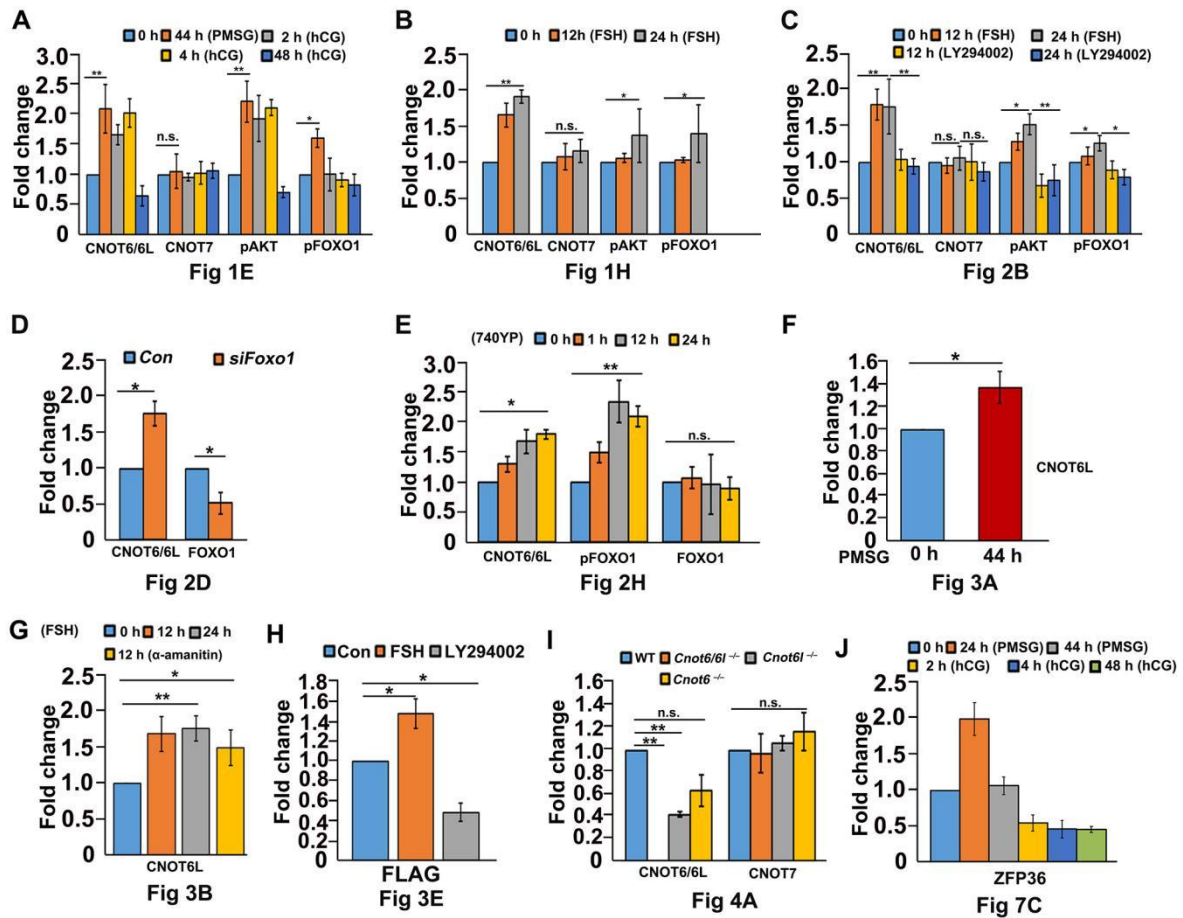


Figure S1, related to Figure 1-7: Quantification of the western blot results in main figures.

- (A) Quantification of the western blot results in Figure 1E.
- (B) Quantification of the western blot results in Figure 1H.
- (C) Quantification of the western blot results in Figure 2B.
- (D) Quantification of the western blot results in Figure 2D.
- (E) Quantification of the western blot results in Figure 2H.
- (F) Quantification of the western blot results in Figure 3A.
- (G) Quantification of the western blot results in Figure 3B.
- (H) Quantification of the western blot results in Figure 3E.
- (I) Quantification of the western blot results in Figure 4A.
- (J) Quantification of the western blot results in Figure 7C.

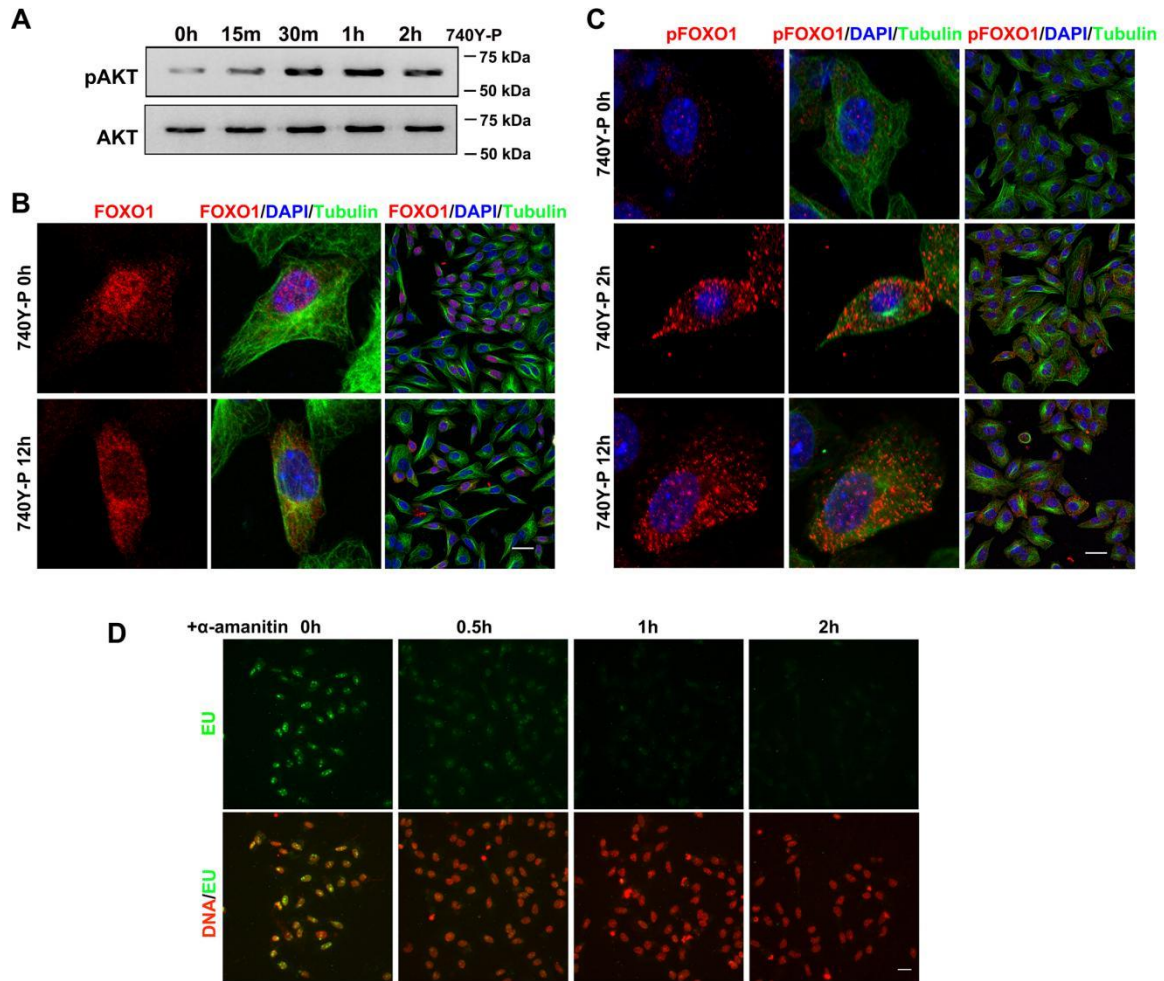


Figure S2, related to Figure 2: Characterization of the effect of 740Y-P and α -amanitin in cultured granulosa cells.

(A) Western blotting of AKT phosphorylation at Ser-473 in granulosa cells treated with 740Y-P (20 nM). AKT was used as a loading control.

(B and C) Immunofluorescence of FOXO1 (B) and phosphorylated FOXO1 at Ser-256 (C) in cultured granulosa cells treated with 740Y-P.

(D) EU staining shows the transcription status of granulosa cells treated with α -amanitin (50 μ M). EU, ethynyl uridine.

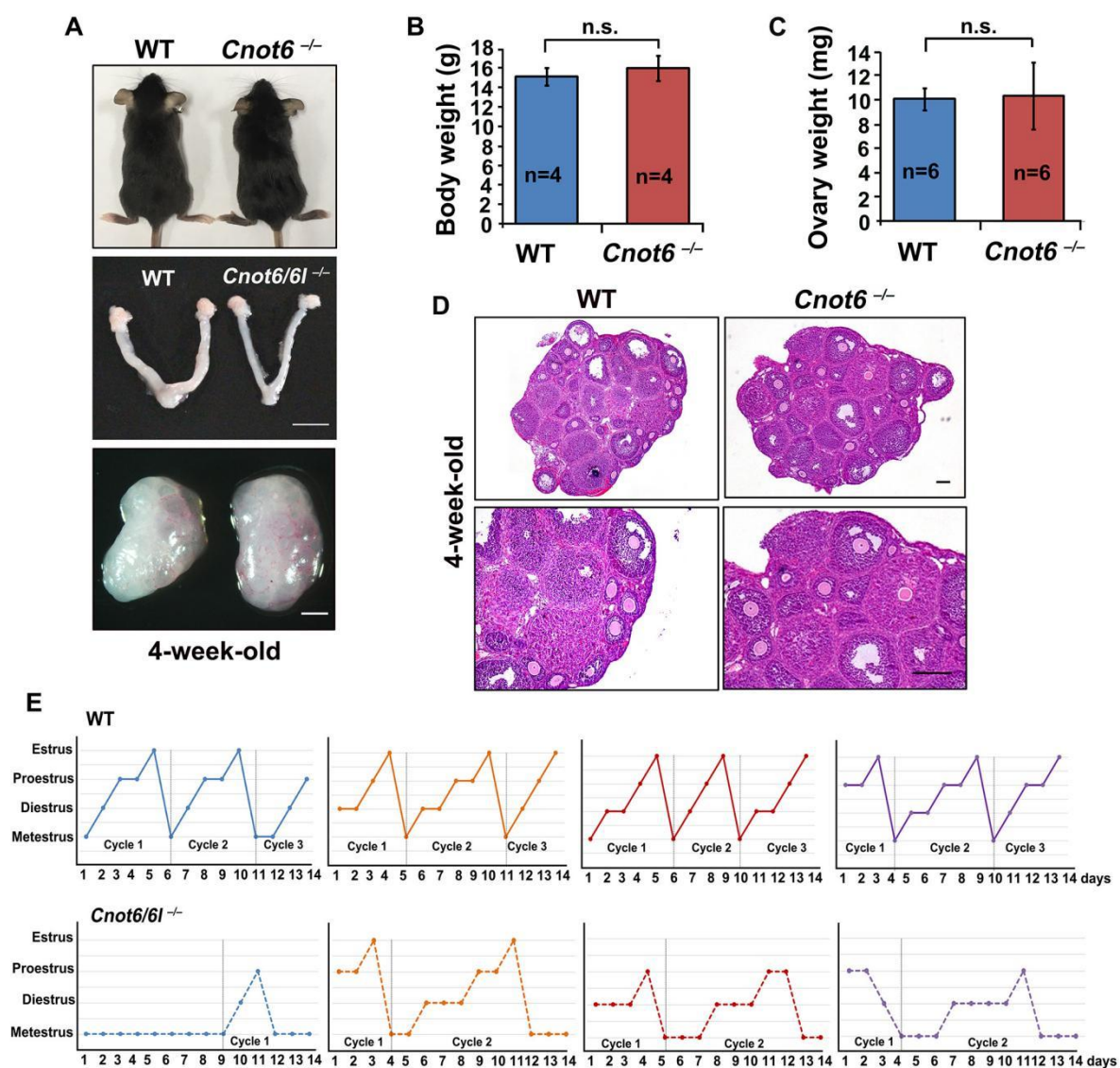


Figure S3, related to Figure 5: Phenotype analyses of the *Cnot6/6l*^{-/-} female mice.

(A) Body size and ovarian morphology of 4-week-old WT and *Cnot6/6l*^{-/-} female mice.

(B) Quantitative statistics of mouse body weight. n = 4 female mice for each genotype. n.s.: non-significant.

(C) Quantitative statistics of mouse ovary weight. n = 6 female mice for each genotype. n.s.: non-significant.

(D) Hematoxylin and eosin staining showing ovarian histology of WT and *Cnot6/6l*^{-/-} mice. Scale bar, 100 μ m. WT, wild-type.

(E) Estrous cycle tests for WT and *Cnot6/6l*^{-/-} female mice. The estrous status of mice at 8 weeks (n = 5 for each genotype) was determined through daily cytology examinations of vaginal cell smears.

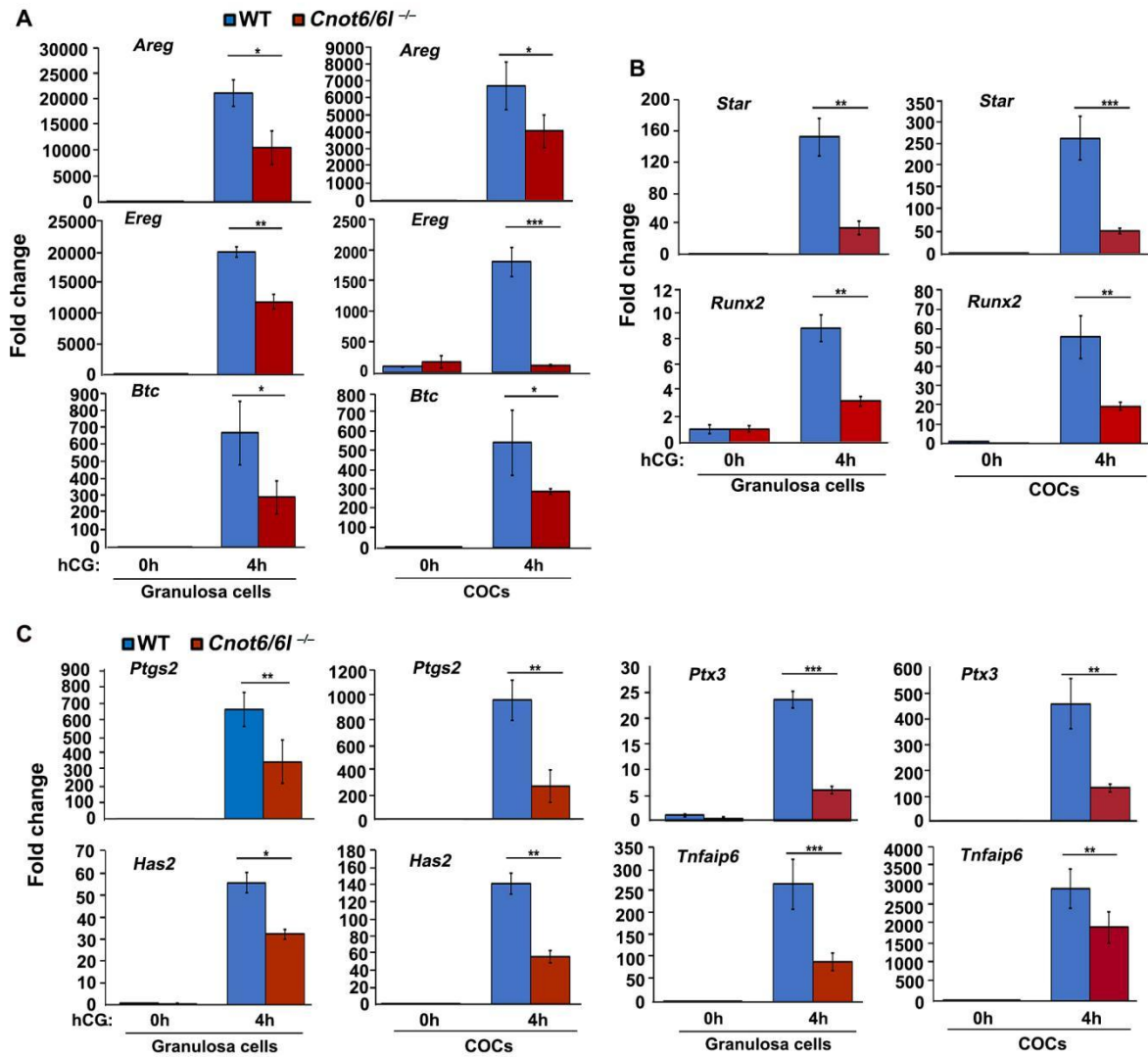


Figure S4, related to Figure 5: Responses of WT and *Cnot6/6l*^{-/-} mice to superovulation treatment.

(A) Quantitative RT-PCR results show the mRNA expression of EGF-like factors (*Areg*, *Ereg*, and *Btc*) in granulosa cells and COCs isolated from WT and *Cnot6/6l*^{-/-} ovaries (0 and 4 h after hCG injection).

(B and C) qRT-PCR results show the expression levels of LH target genes in granulosa cells and COCs isolated from WT and *Cnot6/6l*^{-/-} ovaries (0 and 4 h after hCG injection). Error bars: SEM. *** $P < 0.001$, ** $P < 0.01$, and * $P < 0.05$ according to two-tailed Student's *t*-test.

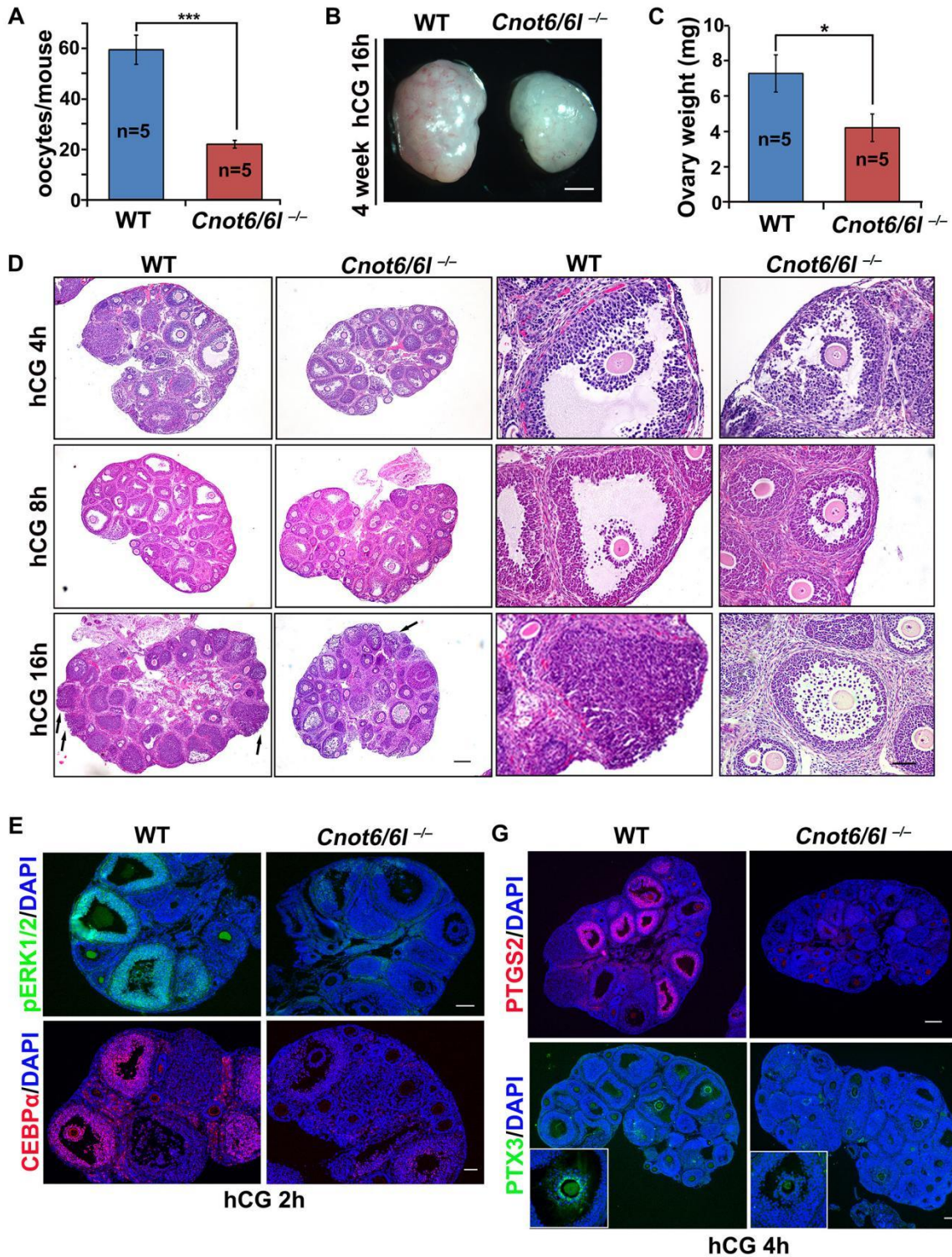


Figure S5, related to Figure 5: Expression levels of LH target genes in granulosa cells and COCs isolated from WT and *Cnot6/6l*^{-/-} ovaries.

(A) Numbers of oocytes ovulated by 4-week WT and *Cnot6/6l*^{-/-} mice 16 h after hCG injection. Five female mice of each genotype (n) were used in this experiment.

(B and C) Representative ovarian images (B) and weights (C) of 4-week-old WT and *Cnot6/6l*^{-/-} female mice 16 h after hCG injection. n: number of ovaries analyzed for each genotype. Scale bar, 500 μ m.

(D) H&E staining results showing ovarian histology of 4-week-old WT and *Cnot6/6l^{-/-}* mice after hCG injection (4, 8, and 16 h). Scale bar, 100 μ m.

(E) Immunofluorescence results for phosphorylated ERK1/2 and CEBP α in the ovaries of WT and *Cnot6/6l^{-/-}* mice at 2 h after hCG injection. Scale bar, 100 μ m.

(F and G) Immunofluorescence results showing the expression of PTGS2 and PTX3 in the ovaries of WT and *Cnot6/6l^{-/-}* mice after hCG injection (4 h). Scale bar, 100 μ m.

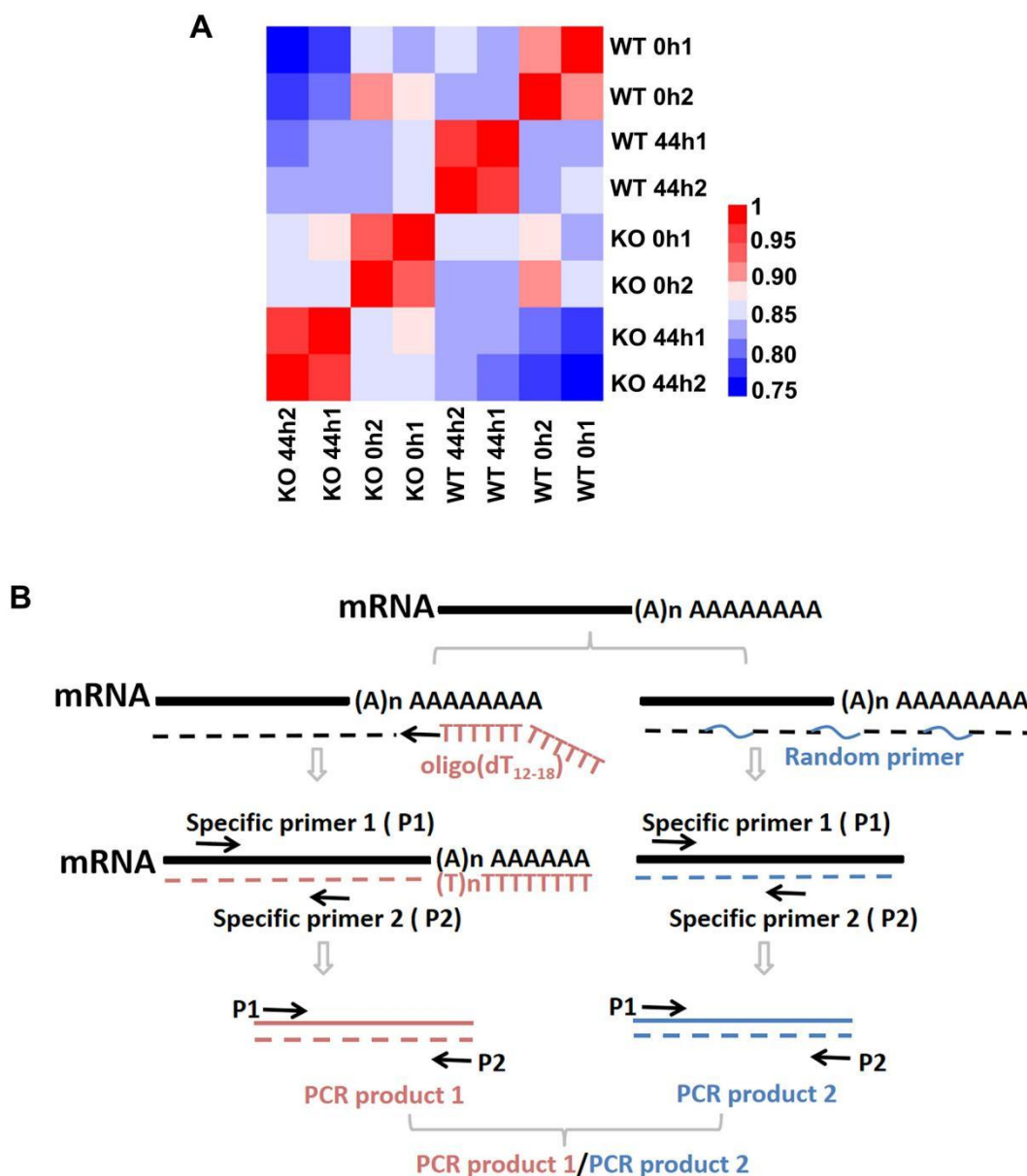


Figure S6, related to Figure 6: Transcript analyses in granulosa cells.

(A) Heatmap of Spearman correlation coefficients of total transcripts among granulosa cells from WT and *Cnot6/6l^{-/-}* mice before and after PMSG injection.

(B) Strategy of the mRNA poly(A) tail length evaluation. The same pool of granulosa cell total RNAs was split and reverse-transcribed using oligo-(dT) and random primers. P1 and P2, gene-specific primers. PSMG, pregnant mare serum gonadotropin; WT, wild-type.

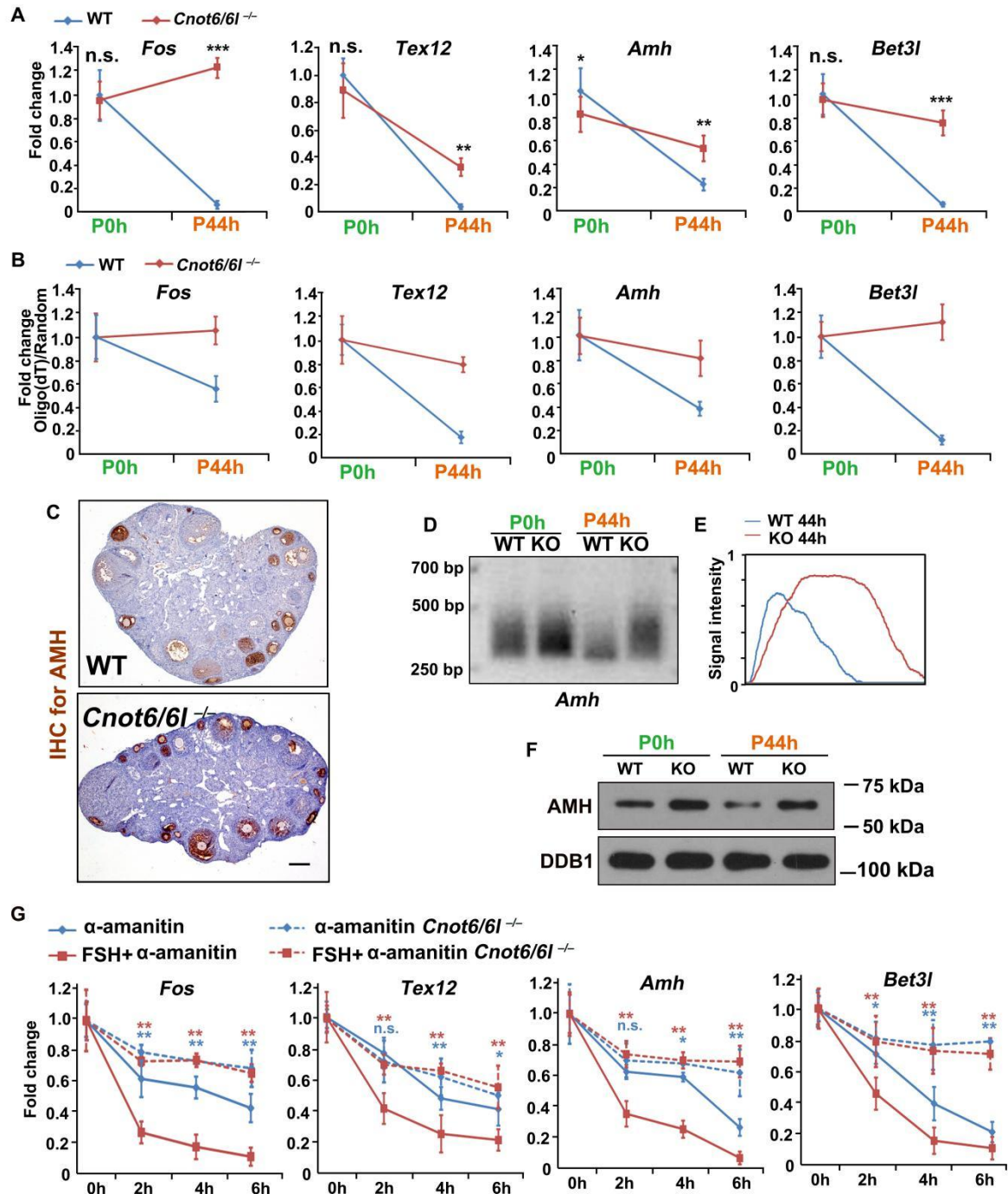


Figure S7, related to Figure 6: Role of CNOT6/6L in regulating mRNA poly(A) tails in granulosa cells.

(A) RT-qPCR results showing the relative levels of indicated transcripts in granulosa cells of WT, *Cnot6/6l^{-/-}* mice 0 and 44 h after PMSG treatment.

(B) Changes of RT-qPCR results obtained from oligo-dT versus random primer-mediated RT reactions reflecting the poly(A) tail length changes of given transcripts in granulosa cells of WT and *Cnot6/6l^{-/-}* mice before and after PMSG treatment.

(C) Immunohistochemistry of AMH in ovaries of 8-week-old WT and *Cnot6/6l^{-/-}* mice. Scale bar, 100 μ m.

(D) Poly(A) tail assay results showing changes in poly(A)-tail length of *Amh* in granulosa cells of WT and *Cnot6/6l^{-/-}* mice before and after PMSG treatment.

(E) PAT assay quantification in (D).

(F) Western blotting shows the expression levels of AMH in granulosa cells of WT and *Cnot6/6l^{-/-}* mice before and after PMSG treatment. Endogenous DDB1 was used as a loading control.

(G) RT-qPCR results showing the changes in indicated transcript levels in cultured WT and *Cnot6/6l^{-/-}* granulosa cells treated with α -amanitin (50 μ M) or FSH (100 ng/mL) plus α -amanitin. Error bars, SEM. Error bars indicate SEM. Data are presented as the mean \pm SEM from at least three independent experiments, one-way ANOVA, * $p < 0.05$, ** $p < 0.01$. n.s.: nonsignificant. PMSG, pregnant mare serum gonadotropin; WT, wild-type; GC, granulosa cell.

Supplementary Tables

Table S1, Related to Figure 6. Spearman correlation coefficients among granulosa cells of WT and *Cnot6/6l*^{-/-} mice 0 and 44 h after PMSG treatment.

Sample	Sample		<i>Cnot6/6l</i> ^{-/-}				WT			
	Stage		44 h		0 h		44 h		0 h	
			1	2	1	2	1	2	1	2
WT	0 h	1	0.76	0.79	0.87	0.85	0.88	0.85	0.91	1.00
		2	0.81	0.83	0.92	0.88	0.86	0.84	1.00	0.91
	44 h	1	0.82	0.83	0.85	0.86	0.96	1.00	0.84	0.85
		2	0.84	0.86	0.85	0.86	1.00	0.96	0.86	0.88
<i>Cnot6/6l</i> ^{-/-}	0 h	1	0.88	0.90	0.95	1.00	0.86	0.86	0.88	0.85
		2	0.87	0.88	1.00	0.95	0.85	0.85	0.92	0.87
	44 h	1	0.96	1.00	0.88	0.90	0.86	0.83	0.83	0.79
		2	1.00	0.96	0.87	0.88	0.84	0.82	0.81	0.76

Table S3, Related to STAR Methods. Primer sequences.

Primer name	Genes targeted	Application	Sequences (5'-3')
<i>Cnot6</i> -qt-F	<i>Cnot6</i>	Real-time PCR	5'-CTCTCGGAGCCTCAAATCCAGT-3'
<i>Cnot6</i> -qt-R	<i>Cnot6</i>	Real-time PCR	5'-TCATTGTACCTCAGTTCCTTGAAGT-3'
<i>Cnot6l</i> -qt-F	<i>Cnot6l</i>	Real-time PCR	5'-CAGCTGTAGTGGAAAGAATGGAAG-3'
<i>Cnot6l</i> -qt-R	<i>Cnot6l</i>	Real-time PCR	5'-CAAGCACGTTTCATATGAGTCTTGG-3'
<i>Foxo1</i> -qt-F	<i>Foxo1</i>	Real-time PCR	5'-GTGAACACCATGCCTCACAC-3'

<i>Foxo1</i> -qt-R	<i>Foxo1</i>	Real-time PCR	5'-TGGACTGCTCCTCAGTTCCT-3'
<i>Cnot6</i> -chip-F	<i>Cnot6</i>	Real-time PCR	5'-GCCCTCGAATGCAGCTATAG-3'
<i>Cnot6</i> -chip-R	<i>Cnot6</i>	Real-time PCR	5'-CCAGTGTCTTGATCTTCCGA-3'
<i>Cnot6l</i> -chip-F	<i>Cnot6l</i>	Real-time PCR	5'-GAACAGGTATGAAGCCTATTC-3'
<i>Cnot6l</i> -chip-R	<i>Cnot6l</i>	Real-time PCR	5'-GGATGGAATTGGGATCTGCA-3'
<i>Fos</i> -qt-F	<i>Fos</i>	Real-time PCR	5'-CGGGTTTCAACGCCGACTA-3'
<i>Fos</i> -qt-R	<i>Fos</i>	Real-time PCR	5'-TTGGCACTAGAGACGGACAGA-3'
<i>Tex12</i> -qt-F	<i>Tex12</i>	Real-time PCR	5'-TGGCAAACCACCTTGTAACC-3'
<i>Tex12</i> -qt-R	<i>Tex12</i>	Real-time PCR	5'-TGCTCATATCGCTCAAATCCTTC-3'
<i>Amh</i> -qt-F	<i>Amh</i>	Real-time PCR	5'-CCCTTCAACCAAGCAGAGAA-3'
<i>Amh</i> -qt-R	<i>Amh</i>	Real-time PCR	5'-GCGGGAATCAGAGCCAAATA-3'
<i>Bet3l</i> -qt-F	<i>Bet3l</i>	Real-time PCR	5'-TGTGCTACTGCAATTGCTCT-3'
<i>Bet3l</i> -qt-R	<i>Bet3l</i>	Real-time PCR	5'-CACTGTCGCCTTTTAGTCTGT-3'
<i>Amh</i> -pat-F	<i>Amh</i>	PAT assay	5'-TACGCGGGCAAGCTGCTCAT-3'
<i>Amh</i> -pat-R	<i>Amh</i>	PAT assay	5'-GCGAGCTCCGCGCCGCGTTTTTTTTTTT T-3'
<i>Zfp36</i> -qt-F	<i>Zfp36</i>	Real-time PCR	5'-TCTCTGCCATCTACGAGAGCC-3'
<i>Zfp36</i> -qt-R	<i>Zfp36</i>	Real-time PCR	5'-CCAGTCAGGCGAGAGGTGA-3'
<i>Zfp36l1</i> -qt-F	<i>Zfp36l1</i>	Real-time PCR	5'-GCTTTCGAGACCGCTCTTCT-3'
<i>Zfp36l1</i> -qt-R	<i>Zfp36l1</i>	Real-time PCR	5'-TTGTCCCCGTACTIONTACAGGCA-3'
<i>Zfp36l2</i> -qt-F	<i>Zfp36l2</i>	Real-time PCR	5'-AGCGGCTCCAGATCAACT-3'
<i>Zfp36l2</i> -qt-R	<i>Zfp36l2</i>	Real-time PCR	5'-CGAAAGCGAAGGCGTTGTTA-3'

Table S4, Related to Figure 6. Quality control of RNA-seq results (granulosa cells of WT and *Cnot6/6l*^{-/-} mice 0 and 44 h after PMSG treatment).

Sample	Total reads	Mapping efficiency
WT-0h-Rep1	29,200,092	90.69%
WT-0h-Rep2	31,193,058	90.57%
<i>Cnot6/6l</i> ^{-/-} -0h-Rep1	35,686,804	90.05%

<i>Cnot6/6l^{-/-}</i> -0h-Rep2	31,356,970	90.67%
WT-44h-Rep1	32,753,938	90.56%
WT-44h-Rep2	30,254,672	89.26%
<i>Cnot6/6l^{-/-}</i> -44h-Rep1	32,569,568	90.35%
<i>Cnot6/6l^{-/-}</i> -44h-Rep1	37,718,484	91.12%